Regional Carbon Fluxes and Boundary Layer Heights from the Airborne Carbon in the Mountains Experiment 2007

by

William K. M. Ahue

A thesis submitted in partial fulfillment of

the requirements for the degree of

Master of Science

(Atmospheric and Oceanic Sciences)

at the

UNIVERSITY OF WISCONSIN - MADISON

2010

APPROVED

Advisor Title:

Ankur R. Desai, Ph.D.

Assistant Professor

University of Wisconsin - Madison

Department of Atmospheric and Oceanic Sciences

_____

Advisor Signature

_____

Date

ABSTRACT

The Central Rocky Mountains, with its abundant forests ecosystem, is likely an important carbon sink with an estimated annual uptake between 57.6 and 80.5 g C m^{-2}. However, ongoing ecosystem stress (i.e. bark beetles, forest fires and drought stress) in the Western United States have added significant uncertainty about the future trajectory of these regional carbon fluxes. Moreover, current regional CO_2 land-atmosphere exchanges are poorly constrained in mountainous regions. Additionally, the evolution of the boundary layer plays an essential role in determining the spatial distribution and vertical mixing of passive tracers and is strongly influenced by orography. To address these issues a field experiment in the Central Rocky Mountains, the Airborne Carbon in the Mountains Experiment, was conducted during the spring and summer of 2007.

Regional surface fluxes of CO_2 were quantified using a boundary layer budget, applied to paired upwind/downwind airborne observations, to determine the relative magnitude of carbon uptake during the 2007 growing season. Mean regional carbon uptake during the experiment was -7.5 μmol m^{-2} s^{-1}. To determine the extent that boundary layer heights affect the uncertainty in boundary layer budget fluxes, three estimates of maximum boundary layer height were obtained. Airborne observations of virtual potential temperature and water vapor mixing ratio, the bulk Richardson number and reanalysis data are used to determine the evolution of the boundary layer over the domain. Uncertainty in the maximum boundary layer height lead to a 26% spread in the regional surface carbon fluxes, computed using the boundary layer budget method, and explained roughly 60% of the variance among them.

The uncertainties in boundary layer budget fluxes are further put into context with continuous observations from the Niwot Ridge Ameriflux Site and results from the CarbonTracker inverse model. All three estimates of regional carbon fluxes show consistency in magnitude but a shift in the timing of peak uptake, ecosystem drought stress and onset of the North American Monsoon. The onset of ecosystem drought stress is showed earliest in the airborne observations while CarbonTracker is the latest.

Multiple parallel profiles were also flown during the experiment in order to capture

the spatial distribution of regional CO_2 caused by complex local flows and large vertical wind shear. The usefulness of this measurement approach and its ability to grasp the spatial distribution of regional CO_2 is examined with a case study using a mesoscale model, RAMS, and a Lagrangian particle dispersion model, HYPACT. Initial results from RAMS show discrepancies when compared to observations, indicating that the current simulation is having problems resolving local flows around the domain. Particle distribution from HYPACT indicate that, although timing of the afternoon flight may be off by a few hours, the measurement approach captures the spatial distribution of regional CO_2 well. These results will help increase our understanding of how forest ecosystems will react to climate change.

ACKNOWLEDGMENTS

Contents

List of Figures

List of Tables

1 Introduction and Background

1.1 Motivation and Research Questions

One of the more heated topics in the political arena is the role of anthropogenic emissions of CO_2 and its effects on climate change. Since the dawn of the industrial revolution, the concentration of atmospheric CO_2 has steadily increased. Analysis of the longest observed record of atmospheric CO_2 concentrations, from Mauna Loa, HI, USA, provides clear evidence of this buildup (*Keeling et al.*, 1976). Further analysis of the time series reveals the seasonal effects induced by the "breathing" biosphere. It is this "breathing" biosphere and its ability to uptake carbon that is the topic of this thesis.

The abundant forest ecosystem of the Central Rocky Mountains is likely an important carbon sink for the Western United States (*Monson et al.*, 2002; *Schimel et al.*, 2002). *Monson et al.* (2002) estimated the cumulative annual carbon sequestration at a forest in the Central Rocky Mountains to be between 57.6 and 80.5 g C m^{-2}. The typical pattern of regional carbon uptake (Figure 1) reveals that spring uptake is modulated by the availability of water from snow melt and reaches a maximum in the early summer months. As plant available water disappears and summer drought stress sets in, the uptake of carbon decreases. Uptake then increases with the onset of the North American Summer Monsoon, reaching a secondary maximum towards the end of fall before decreasing with the onset of winter (*Monson et al.*, 2002).

Ongoing ecosystem stress has added significant uncertainty about the future of regional carbon uptake. These stressors include wildfires and insect outbreaks. Fires play a key role in revitalizing a forest ecosystem by recycling nutrients and maintaining diversity (*Keane et al.*, 2002). However, it stresses the ecosystem by decreasing the available biomass thereby reducing its ability to uptake carbon from the atmosphere. One of the more recent wildfires in the region occurred in 2002 and consumed more than 130,000 acres of land (National Interagency Fire Center, http://www.nifc.gov/). Insects, such as bark beetles, have the ability to cause widespread tree mortality (*Raffa et al.*, 2008). *Kurz et al.* (2008) estimated that the impact from a beetle outbreak in British

Columbia, Canada was equivalent to 75% of the fire emissions from all of Canada from 1959 - 1999. Bark beetles and forest fires are only a few of the many stressors that affect the regional exchange of CO_2 in the Rocky Mountains. Although they are not the scope of this thesis, they are mentioned to show the dynamic balance that ecosystems try to maintain. Changes in the distribution and frequency of these events have the ability to cause the ecosystem to react differently, thereby changing the land-atmosphere exchange of regional CO_2. The effects and inherent variability of these stressors causes CO_2 land-atmosphere exchange in mountainous regions to be poorly constrained in global models, leading to further uncertainty (*Schimel et al.*, 2002). To address these issues in the Central Rocky Mountains, an airborne field campaign was conducted in the region from spring to summer 2007. Details about the field experiment can be found in section 1.4.

The growth and evolution of the atmospheric boundary layer plays a vital role in determining the spatial distribution of CO_2 in mountainous regions (*De Wekker et al.*, 2009; *Sun et al.*, 2010) and is strongly influenced by orography (*Kalthoff et al.*, 1998). Mesoscale circulations such as rotors and upslope winds transport CO_2 from low lying elevations towards mountaintops (*Schimel et al.*, 2002; *De Wekker et al.*, 2009). It is these complex circulations that determines the vertical mixing and exchange of trace gases from the surface to the atmosphere. *De Wekker et al.* (2009) also found that as long as the maximum boundary layer height exceeds mountaintop heights than the growth of the boundary layer has little correlation with the concentration and resulting surface flux of CO_2. Despite this finding three estimates of regional boundary layer heights were obtained in order to assess its influence on the uptake of carbon. The different estimates were chosen for its accessibility, automated procedure or physical representation and are also used to account for the complex boundary layer structure inherent to mountainous terrain. Details about the atmospheric boundary layer and how it behaves in mountainous regions can be found in section 1.3.

There are two strategies used to investigate carbon exchange, each with its own advantages and shortcomings. One approach is based upon inversion of atmospheric CO_2 concentrations. These "top-down" inversions rely on particle transport models to obtain

influence functions and identify source and sink locations. Top-down methods work relatively well on global and continental scales. However, it does poorly at regional and local scales due to the lack of good inflow fluxes, flux of CO_2 advecting into the domain, and the inability of models to account for spatial heterogeneity and local processes. At the other end of the spectrum is the "bottom-up" approach. With this approach, site level measurements are upscaled in time and space, with ecosystem models, to determine the flux of carbon from the surface to the atmosphere. Fluxes obtained using the bottom-up approach are limited by the accuracy and the spatial footprint of the measurement used to obtain them (*Gerbig et al.*, 2009) and the upscaling techniques (*Desai et al.*, 2008).

Atmospheric CO_2 concentrations over the Central Rocky Mountains, collected during the airborne field campaign, are used to obtain a hybrid bottom-up/top-down flux via a boundary layer budgeting technique. This technique is a simple one-dimensional model that computes surface fluxes based upon changes in CO_2 concentrations and relies on the accuracy of the boundary layer height used. These bottom-up fluxes are compared with other regional estimates of carbon exchange. With this in mind, the following questions were asked:

1. What is the relative magnitude of carbon uptake in the Central Rocky Mountains, during the 2007 growing season, compared to an old-growth forest and a shrub wetland?

2. How do flux estimates from the boundary layer budget method compare with those from the Niwot Ridge Ameriflux Site, a flux tower, and CarbonTracker, a continental top-down inversion?

3. How does the uncertainty in boundary layer height affect the fluxes computed using the boundary layer budget method?

4. Does the multiple parallel profiles flown during ACME07 capture the spatial distribution of regional CO_2?

1.2 Other Airborne Regional Carbon Flux Studies

Continental scale fluxes of CO_2 have been studied using global inverse models (*Gurney et al.*, 2002; *Peters et al.*, 2007; *Gourdji et al.*, 2009). Local scale fluxes have been studied using the eddy covariance technique (*Monson et al.*, 2002). Yet, it is non-trivial to infer regional scale fluxes by downscaling from the continental scale or upscaling from local sites (*Gerbig et al.*, 2009). Airborne experiments have been used to develop techniques to close the gap between the fluxes observed on the continental scale with those obtained from local site measurements. Here is a look at some of the recent airborne experiments.

First is an experiment from the Central Amazon near Manaus, Brazil in July 2001. A boundary layer budgeting technique was used to quantify regional carbon exchange over a tropical forest. Fluxes obtained from the airborne measurements were compared with eddy covariance fluxes from two towers. Seven day back-trajectories were computed to identify source locations for air masses arriving at several different heights ranging from 100 to 3000 m above ground level. Regional flux estimates compared well for daytime measurements, but displayed a systematic underestimate of nighttime respiratory fluxes. These results suggest that carbon exchange using eddy covariance measurements overestimate the Amazonian carbon sink (*Lloyd et al.*, 2007).

The CO_2 Budget and Rectification Airborne (COBRA) study, conducted in August 2000, was designed to obtain regional scale carbon fluxes over the United States. The field experiment used back-trajectory Lagrangian particle dispersion model (LPDM) output to determine upwind source locations. Downwind sinks were also sampled in order to obtain receptor based fluxes. The study measured CO_2 concentrations at three different locations across the United States (North Dakota, Wisconsin and Maine). Regional carbon exchange was then computed using a simple one-dimensional boundary layer budget method. The receptor based flux approach was designed to identify processes that could biases flux estimates. This approach also allowed terrestrial, vegetative, and combustion signals to be extracted and analyzed. The spatio-temporal variance of CO_2 concentrations over North America was also characterized (*Gerbig et al.*, 2003*a,b*; *Lin et al.*, 2004, 2007). COBRA-2000 revealed that initial boundary conditions in regional

models induced seasonal biases that propagate as artifacts in the retrieved fluxes (*Gerbig et al.*, 2003*a*), that use of the receptor based approach resolved variations in surface fluxes on scales smaller than the grid of the meteorological fields (*Gerbig et al.*, 2003*b*), that the largest uncertainties were associated with errors in forecasting upstream sampling locations (*Lin et al.*, 2004), and that direct measurements of fluxes from Lagrangian experiments complement surface-based observational sites (*Lin et al.*, 2007).

COBRA was also conducted in 2003 and 2004. COBRA-2000 was designed to link aircraft-derived regional carbon fluxes to tower flux measurements. COBRA-2003 conducted flights over coastal areas in an attempt to characterize the transition of CO_2 as it moves between marine and continental air. COBRA-2004 concentrated almost exclusively on the northeastern part of North America (New England and Québec). Its primary purpose was to establish how well regional fluxes can be constrained in a limited domain with relatively homogeneous terrain and ecosystem type. The intensive field observations obtained from COBRA identified challenges in modeling ecosystem-atmosphere exchanges of CO_2, including the horizontal transport of particles and the extent to which surface fluxes are mixed vertically, and provides an unique data set to test and improve those models (*Lin et al.*, 2006).

The CarboEurope Regional Experiment Strategy (CERES) was developed to estimate the carbon balance over Southwest France. The experiment was performed in Les Landes, France from May to June 2005 and combined airborne and fixed ground measurements to quantify regional carbon fluxes in a 250 x 150 km domain. Initial results found a strong correlation between fluxes of latent heat and CO_2 over the forest but not over agricultural areas suggesting that soil evaporation of arable land contributed more to the overall flux than plant transpiration during the study period. Some agricultural areas appeared to act as a source of CO_2 because it was still in the early stages of development. Footprint analysis of air mass origins indicate that synoptic flows strongly influence the spatial distribution of CO_2 and that mesoscale models are required to accurately resolve the observed tracer gradient (*Dolman et al.*, 2006). CERES was also conducted in April 2007 under wetter soil conditions and an expanded domain. Results from this campaign

were used to constrain ecosystem model parameters including respired CO_2 and leaf area index. CERES showed that it is feasible to obtain a consistent data set of surface and airborne observation of CO_2 fluxes and concentrations and is a first step in improving our understanding of land use and carbon cycle interactions at the regional scale (*Sarrat et al.*, 2009).

1.3 The Atmospheric Boundary Layer in Complex Terrain

The atmospheric boundary layer is the lowest layer in the troposphere that is in contact with the surface of the earth. This direct contact influences its structure due to surface forcing such as frictional drag and heat and momentum transfer. The boundary layer responds on timescales of about an hour. Its thickness can vary from a few meters to several kilometers. The boundary layer is often turbulent and is capped by a stable layer of air above. The turbulence produced in the atmospheric boundary layer is an important mechanism that is responsible for the transport of heat, momentum and passive tracers from the surface to the free troposphere (*Stull*, 1988; *American Meteorological Society*, 2000).

The structure of the boundary layer over land surfaces in high pressure regimes can be divided into three distinct phases. The phases over the course of the day are the mixed layer, the residual layer and the stable boundary layer. In the mixed layer, turbulence is convectively driven and transports heat and momentum vertically. It grows by mixing less turbulent, stable air from above. The residual layer forms shortly before sunset as turbulence decreases. The stable boundary layer forms as the night progresses and modifies the bottom of the residual layer. It is characterized by stable air that suppresses turbulence allowing for the development of cold pools in low lying regions such as valleys and depressions. Boundary layer heights typically are at a minimum during late night and early morning hours, grows as the sun comes up, decreases into the evening hours, and reaches a minimum at night (*Stull*, 1988).

The structure of the atmospheric layer boundary layer over homogeneous terrain is relatively well understood. However, interactions between the surface and the boundary

layer in complex terrain give a different story. In complex terrain, orography strongly influences the growth of the boundary layer and the development of complex mesoscale flows. This dependence decreases during the day as surface heating becomes the driving mechanism (*Kalthoff et al.*, 1998).

Whiteman (2000) identified four phases in the evolution of the boundary layer in mountainous regions (Figure 2). The first phase is the evening phase where the boundary layer is coupled with the atmosphere above it (Figure 2a). As the evening progresses, cold air drains off the mountain leading to the development of downslope winds and the formation of stable valley inversions (Figure 2b). During the night (Figure 2c), the valley boundary layer becomes decoupled from the rest of the atmosphere. Shortly after sunrise, upslope winds develop due to surface heating. These winds transport mass along the sidewalls breaking down the valley inversion that formed during the night(Figure 2d). As the morning continues, more mass and heat is transported up the sidewalls causing a stable core to form in the center of the valley (Figure 2e). To maintain continuity, the stable core is forced to sink. This sinking air warms adiabatically increasing the temperature in the valley and leading to further convection. In the afternoon, the stable core is finally destroyed and the valley circulation becomes coupled with the rest of the atmospheric flow (Figure 2f). This evolution allows CO_2 rich air to be transported from the stable boundary layer to the free troposphere (*De Wekker et al.*, 2009) and facilitates the computation of surface based carbon fluxes. Consequences of the atmospheric boundary layer's structure in complex terrain, as it relates to ACME07, is described in section 1.4.

1.4   Overview of the Airborne Carbon in the Mountains Experiment 2007

The Airborne Carbon in the Mountains Experiment 2007 (ACME07) was an intensive aircraft research campaign that took place from April to August 2007. More than 60 hours of flight time was flown over 18 research flights during 11 flight days. The area of operations spanned a large portion of the Central Rocky Mountains from approximately

37.5^o N to 42.5^o N latitude and 105° W to 109° W longitude (Figure 3). The core sampling period for the research campaign occurred from June to August 2007. This sampling time was chosen to address the various transition periods experienced by Central Rocky Mountain ecosystems.

The field experiment was designed to measure regional surface carbon fluxes through the use of morning upwind and afternoon downwind flight profiles. On each research flight, high accuracy airborne measurements of CO, CO_2, O_2, and H_2O were collected using NCAR instrumentation aboard the NSF/NCAR University of Wyoming King Air aircraft. In addition to these measurements, the standard micrometeorological and radiation observations available on the King Air airplane were also taken. More information about these standard observations can be found at http://flights.uwyo.edu/.

ACME was first conducted in spring to fall 2004 as part of the Carbon in the Mountains Experiment. The goal of this field experiment was to combine both ground and airborne observations over the Central Rocky Mountains to better characterize carbon fluxes in the region. The ground experiment was designed to understand local CO_2 flows, particularly at night where carbon pools exist at low lying elevations, while the airborne experiment was intended to develop techniques to measure regional carbon fluxes in complex terrain as well as its spatial distribution (*Sun et al.*, 2010).

The lessons learned from ACME04 were accounted for and improved upon during ACME07. One of these lessons was that valley cold pools vented later than expected (*Sun et al.*, 2010). This caused the timing of the flights to be shifted towards later hours. Other lessons learned was that complex terrain imparted flux variations and that vertical shear was large in the domain. To resolve the way these influenced the observations, multiple parallel profiles were flown throughout the flight campaign.

ACME is unique because it was conducted in the Central Rocky Mountains. This region presents an area with extremely complex terrain. Not only does the domain vary greatly in elevation, but it also varies in ecosystem type ranging from evergreen forest to deciduous forest to high elevation grasslands and urban areas. These factors affect both the local circulation and spatial distribution of regional CO_2 (*Whiteman*, 2000;

De Wekker et al., 2009; *Sun et al.*, 2010). The multiple parallel profiles used during ACME07 was meant to minimize the uncertainty caused by these factors. The differences from other regional studies and the lessons learned from ACME04 are what makes the ACME07 field campaign distinct.

2 Data and Methods

2.1 Airborne Measurements

This study looked at 14 of the 18 research flights flown during ACME07. The 14 flights span seven flight days (Table 1) where both morning upwind and afternoon downwind profiles were flown and cover the various transition periods experienced by Central Rocky Mountain ecosystems including pre and post peak uptake, drought stress, and onset of the North American Monsoon and the secondary maximum uptake. Flight days were chosen based upon forecast meteorology in conjunction with back-trajectory LPDM output. Days where there was a consensus between particle dispersion output, based upon forecast meteorology, was chosen as a good flight day. Due to the nature of the field experiment, cloudy and low visibility days prohibited flight operations.

Flight planning for the field experiment used a combination of forecast models and two LPDMs in order to select the best profiles to fly. The two LPDMs used was STILT (*Lin et al.*, 2003; *Gerbig et al.*, 2006) and Flexpart-WRF (*Stohl et al.*, 1998, 2005). These LPDMs were combined with various forecast models, at different resolutions, from NOAA NCEP and NCAR WRF. Back-trajectories from five downwind receptor locations (Table 2) were used to determine the upwind flight path which flew multiple parallel profiles to sample across the Central Rocky Mountains (Figure 3) and minimize the effects of vertical shear and flux variations. The sampling strategy for the morning upwind flights was to fly downward approaches from a height above the boundary layer, typically 6000 m above ground level, into valley and mountain areas to within 50 m above the ground. Missed approaches at nearby regional airports were also flown to sample closer towards the ground. For the afternoon downwind flights, spiral descents were flown around each downwind receptor sink location. The idea behind this sampling strategy was to sample both source and sink air masses in order to quantify daytime regional surface carbon fluxes over the Central Rocky Mountains. The approach used to identify receptor air mass source locations is similar to *Gerbig et al.* (2003*b*) and *Lin et al.* (2007). Figure 4 is an example of LPDM output used for flight planning purposes and the actual flight

profiles flown on that day.

Carbon dioxide concentrations were derived using a modified infrared gas analyzer, LOKI, developed at NCAR. This system is based off a commercially available infrared gas analyzer from Li-Cor Biosciences, Inc. Sampled air was pumped into the analyzer from a port located near the nose of the aircraft. This was done to minimize outside contamination. Calibration of the instrument was done during pre- and post-flight using four standard gases. These gases were also periodically pumped into the system in-flight, at multiple altitudes, to account for instrument sensitivity and drift. Voltages measured during flight operations were then converted to CO_2 concentrations based upon cell pressure and temperature and flight meteorological data.

Unforeseen instrument problems during ACME07 caused the accuracy of the LOKI CO_2 measurements to be degraded. Accuracies during initial testing was approximately 0.2 μmol mol^{-1}. However, while in-flight, rapid changes in inertial motion or pressure caused the accuracy to decrease. Even with these precautions, large errors were encountered. After several trials, a spline function was used to fit the calibrations to its known standard. As such, final accuracies for the project ranged from 0.4 to 0.9 μmol mol^{-1} with an mean accuracy of approximately 0.5 μmol mol^{-1}. A secondary CO_2 gas analyzer, the Autonomous Inexpensive Robust CO_2 Analyzer [AIRCOA] (*Stephens et al.*, 2006), was also flown during the August flights. Concentrations from AIRCOA compare well with LOKI for all flights. Therefore CO_2 concentrations from LOKI are used in order to maintain a consistent data set. This error was propagated into the BLB flux calculations along with the uncertainties in Central Rocky Mountain regional boundary layer heights.

In addition to CO_2 concentrations, several of the standard micrometeorological measurements available aboard the King Air are used in this study. These measurements include water vapor mixing ratio, relative humidity, potential temperature, pressure, two-dimensional (horizontal) wind speed, GPS for location corrections and downward looking radar to measure the aircraft's altitude above ground level. Both water vapor mixing ratio and relative humidity are derived from a chilled mirror (Cambridge Systems, Inc.). The chilled mirror, in stable conditions, is accurate to 1° C. A downfall of

the chilled mirror is its slow response time which causes the instrument's accuracy to degrade during rapid changes, especially during accent and decent. Potential temperature is obtained via a reverse flow temperature (Rosemount Analytical, Inc.) and static pressure sensor (Cambridge Systems, Inc.). Both instruments were extremely accurate for the conditions encountered during ACME07. Accuracies for the reverse flow temperature and static pressure sensor were 0.5^o C and 0.5 mb respectively. Wind speed accuracies, based on an inertial reference unit, are close to 1 m s^{-1}. This is also slightly degraded during rapid acceleration periods. The GPS receiver unit flown aboard the King Air aircraft was the Ashtech L1/L2 which is accurate to within a few meters. Radar altitude was obtained with the APN232 radar system and is also accurate to within a few meters. Detailed information about all of these measurements can be found at http://flights.uwyo.edu/.

2.2   Boundary Layer Budget Method

Boundary layer budgets (BLB) provide a method to calculate and interpret surface fluxes (*Betts et al.*, 1992; *Lin et al.*, 2004, 2007; *Lloyd et al.*, 2007). By computing the temporal changes in the scalar concentrations of trace gases (i.e. CO_2), we are able to obtain a surface flux measurement. An extension of the results from *Raupach et al.* (1992) yield the following,

$$F_c = z_{max} \frac{DC_{avg}|_{sfc}^{z_{max}}}{Dt} \tag{1}$$

where F_c is the surface flux (net ecosystem exchange [NEE]), z_{max} is the maximum boundary layer height, and Dt is the time difference between the morning upwind and afternoon downwind flights. DC_{avg} is the difference in the column averaged CO_2 concentration, measured from the surface to z_{max}, from the afternoon to the morning. Negative values of NEE indicate uptake of carbon by the ecosystem while positive values show a release of carbon to the atmosphere. With this form of the equation column averaged variations are not affected by variations in boundary layer height. There are, however, some issues with the method including the ability to track air masses from one domain to another and the accuracy of the boundary layer height used.

Typically z_{max} is written as z_i, or the time varying instantaneous boundary layer height. However, z_{max} is used to calculate the surface flux based upon the following assumptions. *Stull* (1988) and *Garratt* (1990) showed that the convective boundary layer is a vertically confined column of air that incorporates overlaying air into it as it grows. By using z_{max}, we are able to resolve issues with vertical entrainment at the boundary. *Stull* (1988) and *Garratt* (1990) also showed that the bulk properties of the column are independent of small scale heterogeneity, indicating that the convective boundary layer acts as a natural integrator of surface fluxes over complex terrain. Also, *De Wekker et al.* (2009) showed through model simulations with idealized conditions that z_{max} is a good proxy for computing surface fluxes when compared with observations. The multiple parallel profiles, obtained through analysis of the forecast modeled based back-trajectories, were used to account for spatial variations of Central Rocky Mountain regional CO_2 caused by local circulations and large vertical wind shear. The use of z_{max}, in combination with the multiple parallel profiles, affords us the ability to calculate surface fluxes over the domain without requiring detailed spatial maps of z_i.

Parcel trajectory fluxes, based upon receptor LPDM back-trajectories, (Table 2) were also calculated using the BLB method. A receptor is the hypothetical location where particles following a given trajectory, based upon forecast model winds, will end up. It can be viewed as the location where a parcel will reside, when released from a given location and following forecast model winds. In order to compute these fluxes, observations from the flight profiles needed to be paired with its proper receptor. This was done using the LPDM output for each flight day. A least-squares estimate was used to calculate the distance between the flight path and the centroid of each receptor's particles. The centroid is used due to the fact that flights were only flown when there was a consensus between the LPDMs spatial distribution. This least-squares distance was used to partition the morning upwind observations (air mass source) with its afternoon downwind receptor. Due to the sampling strategy used during the afternoon downwind flights a simple box, around each receptor, was used to partition these observations (air mass sink / receptor). The distance threshold used in this study was 10 km. With each receptor's

air mass source and sink location identified, parcel trajectory fluxes could be calculated. The parcel trajectory fluxes are then averaged to obtain a single regional surface flux over the Central Rocky Mountains. By averaging across all receptors, flux variations caused by terrain and large shear are minimized. This was the central idea behind the use of multiple parallel profiles. Domain and parcel trajectory averaged surface fluxes are compared with NEE from NWR (Section 2.4) and CarbonTracker (Section 2.5).

2.3   Determination of Boundary Layer Heights

The boundary layer budget method requires accurate estimates of the maximum boundary layer height. This affects the fluxes calculated by changing the total column height of the air sampled. As such, three estimates of the maximum boundary layer height were obtained for this study. One estimate is from reanalysis model output while the other two use the airborne measurements.

2.3.1   North American Regional Reanalysis Model

One of the estimates of maximum boundary layer height comes from reanalysis model output. Three-hourly surface meteorology from the NCEP's North American Regional Reanalysis (NARR) (*Mesinger et al.*, 2006) model were obtained for 2007. Surface variables were extracted over the ACME domain (Figure 3). Lateral boundaries for NARR are generated via a data assimilation process from NCEP-DOE Global Reanalysis and NCEP Eta model output. This allows the model to obtain the optimal state variables which are consistent with observations. NARR has a horizontal resolution of 32 km. For information about NARR and to download data see http://www.emc.ncep.noaa.gov/mmb/rreanl/.

NARR boundary layer heights were obtained for each flight day analyzed in this study (Table 1). Boundary layer heights are calculated using the Level 2.5 Mellor-Yamada turbulence closure scheme which relies on the dissipation of turbulent kinetic energy (TKE) with height, where z_i is determined once TKE reaches a given threshold. Details about the physics package used in NARR can be found in *Janjić* (1990). For each flight day, boundary layer heights were extracted at 40.13^o N, 107.13^o W. This location was

chosen based upon the flight profiles and represents the center of the domain. Once extracted, the three-hourly boundary layer heights were linearly interpolated to hourly heights. The time evolution of the boundary layer for each day was then analyzed and a maximum height was chosen to be used in the BLB flux calculation.

2.3.2 Parcel Method

The measurement strategy for ACME07 was to fly descending legs from above the boundary layer towards the surface during the morning upwind flights and spiral descents around each receptor during the afternoon downwind flights (Section 2.1). By using this measurement strategy, the aircraft was able to produce vertical soundings. From these soundings, vertical profiles of virtual potential temperature (θ_v) and water vapor mixing ratio (q) were analyzed. θ_v is used to account for density changes caused by moisture. These profiles are averaged into 50 m vertical bins to smooth of the data.

Vertical temperature and moisture profiles provide a quick way to determine the maximum boundary layer height for a given day (*Holzworth*, 1964). In general, the atmosphere can be described as follows. Potential temperature remains relatively constant throughout the mixed layer. Once above the mixed layer the atmosphere becomes stable and potential temperature begins to increase with height. Another characteristic of the mixed layer is its higher moisture content (*Wallace and Hobbs*, 1977). The maximum boundary layer height was determined through visual inspections of the profiles of θ_v and q applied to parcel theory. The height was chosen where the profiles went from well-mixed, cooler and moister air towards stable, warmer, and drier air.

2.3.3 Bulk Richardson Number Approach

The bulk Richardson number (Ri_B) is a common proxy used to determine the atmospheric boundary layer height. It is a dimensionless number that relates vertical stability to vertical shear and represents the ratio between thermally produced turbulence and turbulence produced by vertical shear and is used to identify whether convection is free or forced. The critical Richardson number (Ri_c) is the value of the bulk Richardson

number where the atmosphere switches from unstable flow to stable flow (*American Meteorological Society*, 2000)

The form of the bulk Richardson number used in this study, from *Grimsdell and Angevine* (1998), is

$$Ri_B = \frac{gz\Delta\theta_v}{\overline{\theta_v}[u(z)^2 + v(z)^2]} \qquad (2)$$

where g is the acceleration due to gravity, z is the current altitude above ground level, θ_v is the virtual potential temperature, and u and v are the wind speed components. $\Delta\theta_v = \theta_v(z) - \theta_{vs}$ and $\overline{\theta_v} = 0.5[\theta_v(z) + \theta_{vs}]$, where the subscript s represents surface values. Surface values of u and v are assumed to be zero.

Following the approach described by *Pleim and Xiu* (1995), Ri_c was chosen to be 0.25. The altitude at which Ri_B became greater than Ri_c was chosen as the maximum boundary layer height for that day. The altitude chosen as the maximum boundary layer height varies with the value chosen for Ri_c. Higher values of Ri_c shifted this altitude up while lower values shifted it downwards. *Stull* (1988) suggests that due to the nature of the Richardson number, the critical value chosen is not absolute and depends strongly on the measuring environment and the strength of the turbulence.

2.4 Niwot Ridge Ameriflux Site

The Niwot Ridge (NWR) Ameriflux site (40.05^o N, 105.58^o W) (Figure 3) has been in continuous operation since 1999 and provides standard meteorological measurements in addition to fluxes of CO_2, H_2O, energy and momentum. It uses the eddy covariance technique which relies on high frequency (> 10 Hz) measurements of vertical wind velocity and trace gases to infer surface fluxes. The site is located in a sub-alpine forest ecosystem just below the Continental Divide at an elevation of 3050 m above sea level (*Monson et al.*, 2002). For information about NWR and to download data see http://culter.colorado.edu/NWT/. In this study, half-hourly surface fluxes of NEE were obtained for 2007. These fluxes were averaged for daytime hours (1000 to 1400 LT). This is done in order to compare NEE from NWR with the BLB fluxes from the airborne measurements and also to those obtained from CarbonTracker.

2.5   CarbonTracker Inverse Model

Inverse models have primarily been used to study the effects of CO_2 exchange on the continental scale (*Gurney et al.*, 2002; *Gourdji et al.*, 2009). This is done by constraining prior estimates of surface-atmosphere exchange against trace gas observations. Here, high-resolution (1° x 1°) regional CO_2 fluxes, over the Central Rocky Mountains, from the 2008 release of the NOAA ESRL CarbonTracker (*Peters et al.*, 2007) inverse model are used. CarbonTracker uses atmospheric CO_2 observations from the NOAA ESRL Cooperative Air Sampling network along with modeled transport fields from TM5. Then, though data assimilation, it employs an ecosystem model to obtain the best possible flux parameters. Details about TM5 can be found in *Krol et al.* (2005). For more information about CarbonTracker and to download data see http://carbontracker.noaa.gov.

The ecosystem model contains four modules (fire, ocean, biosphere and fossil fuel). Fire and fossil fuel fluxes are prescribed from existing databases while ocean and biosphere fluxes are adjusted to match observed values from the sampling network. For this study, CarbonTracker biosphere fluxes for 2007 were obtained. These three-hourly fluxes were then interpolated to hourly fluxes and spatially resampled to 0.1^o x 0.1^o. They were then averaged over the entire ACME domain for daytime hours (1000 to 1400 LT). Mean fluxes were also obtained over the footprint of the flights for the seven flight days analyzed (Table 1). The footprint is based upon the northern and southern extent of the morning upwind and afternoon downwind flights (Table 3). The polygon formed by these four corners was used to obtain the estimated daytime (1000 to 1400 LT) CarbonTracker biosphere flux.

2.6   Mesoscale Model Overview

To assess the fidelity of the flight profiles derived from forecast model back-trajectories, we conducted a case study using a mesoscale model and a LPDM. Mesoscale models provide an invaluable tool to study the variability of CO_2 in non-homogeneous terrain. When used in conjunction with observations from mountaintop locations, it affords us an opportunity to assess the ability of these models to simulate complex circulations and

growth of the boundary layer. Both of these factors are important to understand as they both affect the concentration of CO_2 in mountainous terrain. Additionally, LPDMs can be employed in tandem with a mesoscale model to further enhance our understanding of how both of these intricate factors affect the concentration and spatial distribution of CO_2, thereby affecting the flux measured at a given location (*De Wekker et al.*, 2009).

LPDMs allows particles to be transported in the Lagrangian framework rather than in the Eulerian. With the Lagrangian approach, particles of any size and shape can be represented. These particles are maintained in a concentrated plume, particularly near the source location, until atmospheric dispersion indicates that they should broaden. This is in contrast to the Eulerian approach which transports particles from one grid cell to another. With the Eulerian approach, anything smaller than the grid spacing is unable to be resolved (*Walko et al.*, 2007). Therefore, a LPDM allows non-diffusive passive traces to be tracked in contrast to the Eulerian approach which computes grid cell particle concentrations.

2.6.1 RAMS Description

The mesoscale model used is the Regional Atmospheric Modeling System (RAMS), Version 6.0 (*Pielke et al.*, 1992; *Cotton et al.*, 2003). Surface-atmosphere processes are represented by the Land Ecosystem Atmosphere Feedback Model, Version 2 (*Walko et al.*, 2000) with eight levels in the ground (up to 1 m deep). Surface fluxes of heat, momentum and water vapor are calculated using the Louis scheme in which the computed fluxes serve as the lower boundary for the sub-grid diffusion scheme for the atmosphere. Turbulence closure is computed using the Mellor-Yamada 1.5 order scheme. For a more complete description of RAMS, see *Pielke et al.* (1992) and *Cotton et al.* (2003). The technical manual for RAMS, Version 6.0 can be found at http://www.atmet.com/index.shtml.

The model domain consist of one grid centered at 40° N, 106.5^o W. The grid covers a large portion of the Colorado Rocky Mountains [415.5 x 366 km] (Figure 5) and has a horizontal grid spacing of 1500 m with 277 grid points in the East-West direction and 244 grid points in the North-South direction. The grid has 45 vertical levels with a grid

spacing of 50 m near the surface. Vertical grid spacing increases by a factor of 1.09 with increasing levels, with a maximum grid spacing of 1000 m at the model top. The top of the model is at 19 km with the first model level, above ground, at 24.5 m. Topography and vegetation cover are derived from the United States Geological Survey 30 arc-second (approx. 1 km) digital elevation model. The simulation is for 21 June 2007, and starts at 0600 UTC (2300 MST, 20 June 2007). The simulation is run for 18 hours and ends at 22 June 2007 at 0000 UTC (1700 MST, 21 June 2007). Initial and boundary conditions of the five outer most grid points were nudged towards NCEP reanalysis output at three hourly intervals to allow for changes in large-scale circulation which might influence the model simulation.

2.6.2   HYPACT Description

The LPDM used to simulate particle dispersion is the Hybrid Particle and Concentration Transport Model (HYPACT), Version 1.5 (*Walko et al.*, 2007). HYPACT is driven by the RAMS model output described in section 2.6.1 and simulates the dispersion of atmospheric tracers under the influence of winds and turbulence. It allows for the assessment of the impact of multiple sources emitted into complex terrain. A recent application of of HYPACT in complex terrain can be found in *De Wekker et al.* (2009).

HYPACT was run for the same flight day as the RAMS simulation, 21 June 2007. Five source locations (Figure 5 and Table 4) were chosen based upon the footprint of the morning research flight and are located at the furthest upwind points sampled. The sources are point features that are located 100 m above ground level. HYPACT was set to release 1000 particles from each source location in an instantaneous burst at 1500 UTC, the closest time step to the start of the morning upwind flight. Particles are then tracked until the end of the simulation at 0000 UTC, 22 June 2007. This approach was designed to evaluate the measurement strategy used during ACME07 and to see whether the field campaign was successful in chasing air masses from one domain to another.

3   Results

3.1   Evaluation of RAMS and HYPACT Simulations

A case study was preformed for 21 June 2007 to evaluate the measurement strategy and test whether the experiment successfully chased air masses from one region to another. This was done using a mesoscale model, RAMS, in tandem with a LPDM, HYPACT. The RAMS simulation ran for 18 hours and started at 0600 UTC on 21 June 2007. This day was characterized by clear skies with weak southwesterly synoptic flows. A low pressure center (1009 mb) was located near the Colorado and Nebraska border.

RAMS model output show some discrepancies when compared with observations from NWR. Observations (solid line) of temperature (Figure 6, top left) and wind speed (Figure 6, bottom left) compare well with model output (dashed line) during the times of the morning upwind and afternoon downwind flights, after 1500 UTC. The model tends to underestimate water vapor mixing ratio (Figure 6, top right) by a factor of two throughout the simulation and shows a shallower diurnal cycle for temperature. Wind directions (Figure 6, bottom right) compare well during early hours, but diverge after 1500 UTC where the model shows a shift towards easterly winds. Observed wind directions do shift towards southerly winds before returning to westerlies. The mismatch between observations and model output at NWR indicate that the current simulation is having problems resolving local flows around the area. Other reasons for the mismatch could be that model forcing may not be properly parameterized or that the NECP reanalysis output used to account for large scale circulations is not correct. To see what is causing the mismatch between observations and RAMS model output, further simulations need to be preformed to get model parameters to match with observations.

Another way to evaluate the model's performance is to compare it with upper air measurements. For this, model output at 1200 UTC, 21 June 2007 is compared with the 12Z upper air sounding from the Denver International Airport, USA [ICAO: KDEN] (Figure 7). Observations (solid line) from the Denver sounding compare well with model output (dashed line). The temperature profile (Figure 7, top left) compares well, but

the model is slightly warmer throughout the column. Modeled dew point temperature (Figure 7, top right) are slightly cooler from the surface to around 5 km where it becomes warmer than observations. Wind speeds (Figure 7, bottom left) up to 1 km show an inverse relationship. Above 1 km, modeled and observed wind speeds compare relatively well. Wind direction (Figure 7, bottom right) compares well from the surface to 14 km. Both observations and model output show a shift in wind direction, but the model shows this shift higher. The correlation between model output and the Denver sounding indicate that synoptic flows are correctly modeled and that issues involving the mismatch at NWR are caused by complex local circulations.

HYPACT is used to determine whether the experiment was able to follow air masses around the domain. Particles were released from five upwind sources (Table 4) and transported under the influence of the RAMS simulation. Each source, a point feature located 100 m above ground level, released 1000 particles at 1500 UTC (Figure 8, top left). At this time the morning upwind flight just took off from Laramie, WY, USA and particles are located near the source. At 1800 UTC (Figure 8, top right), shortly before completion of the morning flight (blue line), the particles have advected towards the northeast, downwind of their source location. Two hours later at 2000 UTC (Figure 8, bottom left), 30 minutes before takeoff of the afternoon downwind flight, particles are still being transported towards the northeast but have begun to spread out. At the completion of the afternoon flight (green line) at 0000 UTC, 22 June 2007 (Figure 8, bottom right), the particles, still traveling towards the northeast, have started to merge with one another. Based upon these results, timing of the upwind flight is off by a few hours and that the afternoon downwind flight should have left Laramie, WY, USA later. The flight profile could have also been shifted towards the west, to account for the spatial variability of the particle distribution, but this would have negated parcel trajectory flux calculations, based upon receptor LPDM back-trajectory output. These results could change with further RAMS simulations. Nonetheless, the measurement strategy did a good job at following air masses around the domain due to the close resemblance between the particle distribution and flight profiles. Therefore, the multiple

parallel profile approach was able to capture the inherent spatial variability of regional CO_2 in the Central Rocky Mountains and gives confidence in the ability of the BLB method to calculate regional surface fluxes.

3.2   Regional Boundary Layer Heights

Three estimates of daily maximum boundary layer height were obtained for use in the BLB method (Equation 1). These estimates affect the flux calculated by changing the total column height of the air sampled and used in the computation. The maximum boundary layer heights are estimated from reanalysis model data and airborne measurements.

Reanalysis boundary layer heights were obtained from NARR (Table 5). These heights are computed via the TKE method which relies on the dissipation of turbulent kinetic energy with height (Section 2.3.1). Boundary layer heights were extracted at 40.13^o N, 107.13^o W. Boundary layer heights were extracted from a single grid cell in the center of the domain, based upon the flight profiles. Heights around this grid cell are different and sensitive to the local orography. The average maximum NARR boundary layer height, among all flight days, was 3198 m with a standard deviation of 696 m. Figure 9 shows the evolution of the boundary layer on 21 June 2007. The maximum boundary layer height on this day was 4551 m. From 0000 to 1200 Local Time [LT] (0700 to 1900 UTC) the top of the boundary layer oscillates between 1000 m and 2200 m. After 1200 LT, the boundary layer grows steadily till it reaches a maximum at 1500 LT. It begins to decay at 1800 LT, reaching a minimum at 2100 LT (0400 UTC). The evolution of the boundary layer on the remaining flight days show a similar pattern with low heights from 0000 LT till around 1000 LT. As daytime heating increases, the boundary layer being to grow till it reaches a maximum around 1600 LT. It remains constant for a few hours and then begins to decay, reaching a minimum around 2200 LT.

Boundary layer heights were also estimated using parcel theory (Table 5). Visual inspection of the vertical profiles of θ_v and q, along with parcel theory, was used to estimate the daily maximum boundary layer height. The average height among all flight

days was 2867 m with a standard deviation of 422 m. Figure 10 shows the vertical profiles of θ_v and q on 21 June 2007 from the morning upwind (green) and afternoon downwind (red) flights. The stable morning boundary layer height was approximately 500 m with a maximum height during the afternoon of 3574 m. These profiles are a classic example of parcel theory. In the mixed layer, the profile is well mixed, cooler and moister. Once above the mixed layer the profile becomes stable, warmer and drier.

The final estimate was computed using the bulk Richardson number approach (Equation 2). A critical value of 0.25 was used (*Pleim and Xiu*, 1995). The altitude where Ri_B became greater than Ri_c was chosen as the maximum boundary layer height (Table 5). Figure 11 shows the vertical profiles of Ri_B on 21 June 2007. Ri_B was averaged into 50 m vertical bins. The morning upwind profile (green) has a boundary layer height of 1801 m. The maximum boundary layer height, from the afternoon downwind profile (red), was 3648 m. This is about 900 m lower than the height extracted from NARR and about 100 m higher than the one obtained from parcel theory. On this day, a Ri_c value of 0 yields a maximum boundary layer height of 3596 m while a Ri_c value of 1 gives a height of 3648 m. The average height from the bulk Richardson number approach was 2571 m with a standard deviation of 1152 m.

There are strong correlations among the three estimates. Correlations coefficients range from 0.76 between NARR and the bulk Richardson Number approach to 0.96 between NARR and parcel theory. The correlation between the bulk Richardson number approach and parcel theory is 0.82. There are some similarities among the different flight days (Figure 12). Estimates from the bulk Richardson number approach generally yield the lowest height. NARR boundary layer heights are typically the highest. On some days, NARR compares extremely well with the bulk Richardson number approach. On others it compares well with parcel theory. There are a few days with large differences between the bulk Richardson number approach and the remaining estimates, where the height is approximately 1000 m lower. On 21 June 2007, the NARR maximum boundary layer height is approximately 900 m higher than the other two estimates. The uncertainty in boundary layer heights from NARR is 36%, based upon the 1-σ spatial variability. The

bulk Richardson number approach has an uncertainty of 25%, computed by changing the critical Richardson number and the altitude bin size. Parcel theory yields the smallest uncertainty, 4%. The error for parcel theory boundary layer heights was computed by changing the bin size and averaging scheme. As a result, computed error was twice the bin size, 100m. Instrument error was negligible. The combined uncertainty for all three estimates is 25%.

3.3   Regional Carbon Fluxes

Regional carbon fluxes from ACME07 (Table 6 and Table 7) were computed using a boundary layer budgeting technique (Equation 1). The fluxes vary depending on the height used in the computation. BLB fluxes were computed using three height estimates to see what affects it may have. The sampling strategy used during ACME07 also allowed for the computation of parcel trajectory fluxes, based upon receptor LPDM back-trajectory output. By computing a least-square distance from the morning flight path to the centroid of the particles released from five downwind receptors and sampling around these receptors during the afternoon upwind flight, air mass source and receptor sink locations were able to be identified. These parcel trajectory fluxes are then averaged together to minimize spatial variability and was the central idea behind the use of multiple parallel profiles. In addition to the BLB fluxes calculated, daytime averaged fluxes from NWR and CarbonTracker and footprint fluxes from CarbonTracker were also obtained. These are used to qualify the BLB fluxes from ACME07.

Daytime averaged fluxes from NWR (Figure 13, solid line) shows strong uptake of CO_2 in late spring to early summer with a maximum uptake near -12 μmol m^{-2} s^{-1}. This is followed by a decrease in uptake during the mid-summer due to ecosystem drought stress. Uptake of CO_2 increases slightly in the late summer period as rain fall increases due to the onset of the North American Monsoon. Daytime and domain averaged CarbonTracker fluxes (Figure 13, dot-dashed line) display a similar pattern. However, timing of peak uptake and drought stress are shifted towards later in the summer. BLB fluxes (Figure 13, circle), computed using the maximum boundary layer height from parcel theory, shows

broad agreement when compared with NWR and CarbonTracker but indicates an earlier onset of late-summer ecosystem drought stress. The patterns and magnitudes among all three estimates of daytime regional surface carbon fluxes are consistent with one another.

BLB fluxes were computed using three estimates of maximum boundary layer height (Figure 14 and Table 6) from NARR reanalysis data (Figure 14, circle), parcel theory (Figure 14, square) and the bulk Richardson number (Figure 14, triangle). There is strong agreement among all flux estimates, with the exception of one flight day, 3 August 2007. On this day, the BLB flux computed using the bulk Richardson number maximum boundary layer height shows a release of carbon to the atmosphere. Correlation coefficients among the three estimates range from 0.9 between NARR and parcel theory boundary layer heights to 0.8 when you compare with flux estimates using the bulk Richardson number boundary layer heights. Mean BLB flux, for NARR boundary layer heights, is -7.3 μmol m^{-2} s^{-1} with a standard deviation of 3.5 μmol m^{-2} s^{-1}. Mean BLB flux, obtained via parcel theory boundary layer heights, is -6.6 μmol m^{-2} s^{-1} with a standard deviation of 2.8 μmol m^{-2} s^{-1}. Mean BLB flux, computed from bulk Richardson number boundary layer heights, are -6.0 μmol m^{-2} s^{-1} with a standard deviation of 4.4 μmol m^{-2} s^{-1}. Estimates obtained using parcel theory boundary layer heights have the smallest uncertainty due to the fact that the boundary layer height used is the most physically represented while those obtained via bulk Richardson number heights show the smallest uptake and are the most uncertain. Mean BLB fluxes from NARR heights indicates the greatest uptake.

The measurement strategy used during ACME07 facilitated the computation of parcel trajectory fluxes (Table 2). Upwind receptor source locations were computed using a least-squares distance between the centroid of the released particles and the morning flight path. Downwind receptor sinks were computed by taking a box around each receptor. With each receptor's air mass source and sink locations identified, parcel trajectory fluxes are calculated using the BLB method (Equation 1). The receptors used for this process run along a North-South line near the continental divide (Figure 3). There is significant variability among the receptor's mean flux. The Willow Creek receptor shows the greatest

uptake, -13.2 μmol m^{-2} s^{-1}, while both the Granby and Walden receptor have the least uptake, -1.2 and -1.6 μmol m^{-2} s^{-1} respectively. There is no gradient along the North-South line of the receptors.

Multiple parallel profiles were flown throughout the experiment to minimize the uncertainty in regional surface fluxes caused by local circulations and the spatial distribution of CO_2. The multiple parallel profiles were meant to sample across the upwind receptor source locations. By averaging across all receptors (Table 7), flux variations caused by these local process are accounted for. Comparison between the average BLB receptor flux and the domain BLB flux, computed using parcel theory boundary layer heights, shows a strong relationship (Figure 15). The correlation between the two is 0.8. A linear regression was computed using these flux estimates. Results from the regression gives a slope of 0.7 (dot-dashed line). A majority of the flight days (5 of 7) compare well with one another and have close to a one-to-one relationship, within the uncertainty of the BLB estimates. For the remaining flight days, the receptor averaged BLB flux shows greater uptake than the domain BLB flux. There is no temporal pattern for when the receptor averaged BLB flux has greater uptake. Removing these two flight days indicates a strong correlation, $R = 0.9$, and a slope of 0.9.

Average BLB receptor fluxes, computed by averaging across the five receptors for each flight day, are put into perspective by computing CarbonTracker biosphere fluxes averaged over the footprint of the morning upwind and afternoon downwind flight profiles (Table 3) during daytime hours. The CarbonTracker footprint fluxes (Figure 16, triangle) show a similar pattern and magnitude as receptor averaged BLB fluxes (Figure 16, circle) and daytime averaged fluxes from NWR (Figure 16, square). As noted earlier, BLB fluxes display an earlier onset of summer ecosystem drought stress. CarbonTracker shows the latest onset of this stress. Although all estimates display a similar pattern and have similar magnitudes, there is little similarity between them. The strongest correlation is between receptor averaged BLB fluxes and NWR daytime averaged flux, $R = 0.3$. NWR daytime averaged fluxes and CarbonTracker footprint fluxes show no correlation with one another, $R = 0.1$. CarbonTracker footprint fluxes display an inverse relationship when

compared with receptor averaged BLB fluxes, $R = -0.2$. However, a further look at the fluxes indicates two periods. The first period contains the first three flight days, with the second period containing the remaining flights. A linear regression during the first period gives an extremely shallow slope of 0.10 but strong correlation, $R = 0.9$. For the second period, linear regression gives a slope of 0.60 but a weaker correlation, $R = 0.7$. Further analysis of CarbonTracker is required to identify the reason(s) behind the two periods indicated by these results which are possibly related to problems using global inversions in a regional context including inverted diurnal cycles based upon negative scaling factors for some eco-regions. Additionally, the small sample size used likely have statistical artifacts in them. Further measurements are needed to see if the correlation values are statistically significant. Despite these results, each estimate represents an independent measurement and there is no evidence that suggest that site measurements represent more than just a single site or that global inversions can be used to obtain regional estimates. The BLB fluxes are meant to characterize regional carbon exchange and the similarity in pattern and magnitude among the different estimates suggest that both site measurements and global inversions can be used to quantify regional CO_2 land-atmosphere exchanges.

4 Discussion

Regional carbon fluxes, over the Central Rocky Mountains (Figure 3), were estimated using three distinct methods. Daytime averaged fluxes from NWR, which relies on the eddy covariance technique, had a mean uptake of -5.6 μmol m^{-2} s^{-1} over the seven flight days. Fluxes obtained from the CarbonTracker footprint analysis, which uses observations and an inverse model to constrain prior fluxes, have a mean uptake of -7.0 μmol m^{-2} s^{-1}. BLB fluxes, computed using a boundary layer budgeting method and airborne measurements from ACME07, had a mean uptake of -7.5 μmol m^{-2} s^{-1}. All flux estimates show a similar pattern but the timing of peak uptake, ecosystem drought stress and the onset of the North American Monsoon are offset from one another. BLB flux estimates indicate the onset of ecosystem drought stress the earliest while CarbonTracker shows this to be later in the summer. Results from this analysis suggest that the Central Rocky Mountains is an important carbon sink for the Western United States. Further understanding of ecosystem-atmosphere exchange of trace gases and how it will be impacted by climate change remains an important scientific question that need to be addressed further.

There are complications involved with comparing Central Rocky Mountain regional flux estimates from different methods. There is no reason why they should compare well with one another due to the different techniques and footprints used to obtain each estimate. NWR fluxes are obtained from a canopy tower that has a spatial fetch of approximately 1 km. Its flux is representative of the forest around the site, but should not be representative of regional uptake. CarbonTracker fluxes have a spatial resolution of 1° x 1° and are not meant for regional studies. Its temporal and spatial resolution is too coarse. To obtain a decent estimate of regional carbon fluxes using CarbonTracker, one needs to average fluxes across eco-regions. In contrast, BLB fluxes only flew during daytime hours. However, it flew over a large area and the measurement obtained give the best possible representation of carbon uptake over the entire domain. In spite of these complications, the strong similarities in pattern and magnitude bring to light the fact that BLB and NWR flux uncertainties can be used to constrain the uncertainty in

CarbonTracker and further narrow down the scale of regional carbon uptake.

To get an idea of how much information is gained by ACME07, BLB fluxes are compared with fluxes from a shrub wetland in North Central Wisconsin (Lost Creek) and a predominately red oak and red maple forest in rural New England (Harvard Forest). NEE from Lost Creek have a peak uptake near -2.9 μmol m^{-2} s^{-1} over a six year period with a yearly average of -0.22 μmol m^{-2} s^{-1} (*Sulman et al.*, 2009). This is in contrast to Harvard Forest, which had summertime mid-day NEE between -20 and -30 μmol m^{-2} s^{-1} (*Goulden et al.*, 1996). Receptor averaged BLB fluxes, from ACME07, have a mean uptake of -7.5 μmol m^{-2} s^{-1} with a standard deviation of 3.5 μmol m^{-2} s^{-1}. While BLB fluxes do not show as much uptake as the old-growth Harvard Forest it does reveal greater uptake than Lost Creek. Regional flux estimates from COBRA were -1.6 to -3.8 μmol m^{-2} s^{-1} for North Dakota, USA, -1.7 to -3.3 μmol m^{-2} s^{-1} for Wisconsin, USA, and -15 μmol m^{-2} s^{-1} over Maine, USA (*Lin et al.*, 2004). Regional estimates from CERES ranged from -15 μmol m^{-2} s^{-1} over forested regions to -3 μmol m^{-2} s^{-1} over agricultural areas (*Dolman et al.*, 2006). CarbonTracker mean summer time flux over all of North America was -5.2 Pg C yr^{-1} (-0.60 μmol m^{-2} s^{-1}). Therefore, any information gained during ACME07 will further help to narrow down the uncertainty in carbon sequestration across the Continental United States by providing a dedicated data set that can be used to constrain ecosystem models and regional inversions.

Regional boundary layer heights were obtained through a variety of methods. The accuracy of these heights affects the surface fluxes calculated using the BLB method by changing the total column height of the observations used. As such, a maximum boundary layer heights for each flight day was obtained from reanalysis data, parcel theory and the bulk Richardson number. The mean height from the three methods was 3198 m for NARR, 2867 m for parcel theory and 2571 m for the bulk Richardson number. All three estimates seem to be quite large at first glance. However, *Holzworth* (1964) showed that summertime conditions in the Rocky Mountains typically produce maximum boundary layer heights that exceed 3000 m above ground level. This was done using 10 years of radiosonde data from 45 stations across the contiguous United States. Parcel theory

was applied to mean temperature profiles at each station and mean mixing depths were obtained. *Holzworth* (1964) concluded through his analysis that mean summertime mixing depth were virtually unlimited over the Rocky Mountains. *De Wekker et al.* (2009) also showed that as long as the maximum boundary layer height exceeds mountaintop heights, the growth of the boundary layer bears little correlation with the concentration of CO_2 at a mountaintop location. The average height of the Colorado Rocky Mountains is 3050 m. However, since all heights used in this are measured from above ground level, the maximum boundary layer height chosen exceeds the mountain top heights. Because of this, fluctuations in the growth of the boundary layer and CO_2 concentrations will only have a small affect on the surface flux calculated and explains the strong correlation among the different BLB fluxes.

The uncertainty for the various estimates of maximum boundary layer height ranged from 4% for parcel theory to 36% for NARR. The bulk Richardson number approach had an uncertainty of 25%. The combined uncertainty for all three estimates was 25%. This uncertainty in maximum boundary layer height lead to a 26% spread in the BLB fluxes and explains roughly 60% of the variance among the different estimates. Boundary layer heights obtained via parcel theory and visual inspections of the vertical profiles of θ_v and q provided the least uncertain heights are are the most physically based. By averaging multiple descent profiles the method was able to obtain a general representation of regional boundary layer heights in the Central Rocky Mountains during the times of the flights, neglecting convective plumes and latent heat fluxes. This is in contrast to the estimates obtained from NARR. NARR boundary layer heights were extracted from a single grid point in the center of the ACME07 domain. This location was chosen for its ease and the evolution at one grid point should not be the same as the next and that this, or any other, grid point provides a good representation of Central Rocky Mountain regional boundary layer heights. Despite this downfall, as long as the maximum boundary layer height exceeds the height of mountaintops it will only have a small affect on the surface fluxes computed (*De Wekker et al.*, 2009). This is in contrast to equation 1 which suggest that the two are linearly related.

An issue with the estimates obtained from the bulk Richardson number approach is that it can be skewed depending on the value chosen for Ri_c. Therefore, a set value for the critical Richardson number is not always the best approach. The measuring environment and strength of the turbulence needs to be accounted for (*Stull*, 1988). Yet choosing a critical Richardson number that varies by day is non-trivial. To test this issue, several values of Ri_c were used ranging from 0 to 1. The test found that when $Ri_c = 0$, the maximum height shifted down an average of 100 m. With a Ri_c value of 1, the maximum height shifted up, but only a few meters. This simple test showed that a Ri_c value of 0.25 is appropriate for the conditions encountered during ACME07. Although the bulk Richardson number approach had a large uncertainty associated with it, it does give a decent representation of regional boundary layer heights because it uses the airborne measurements. The automated procedure behind the method makes the bulk Richardson number approach useful because it is easy to implement. Also, as long as the maximum boundary layer height exceeds the top of the mountains, it will yield similar surface fluxes.

The measurement strategy used during ACME07 enabled the computation of parcel trajectory fluxes, based upon receptor LPDM back-trajectory output. By using multiple LPDMs and forecast models at various resolutions, the field experiment was able to identify optimal areas in order to obtain a representative sample of the spatial distribution of regional CO_2. With upwind receptor source locations identified and sampled and receptor sinks sampled, the uptake of carbon at a given receptor was computed. The use of multiple parallel profiles and averaging across the North-South line of the receptors allowed for flux variations caused by complex terrain and large vertical shear to be minimized. The downfall behind computing parcel trajectory fluxes is the ability to correctly identify and partition the upwind source locations, something that is not needed when computing the flux over the entire domain. Here, a least-squares distance was computed from the flight profile to the centroid of the released particles. The centroid was chosen because flights were only conducted when there was a strong consensus between the LPDM particle distribution. However, the LPDM results used to compute this distance

is from forecast model output. To see whether this output is representative of the day, further simulations need to be obtained and analyzed. This can be done through the use of Monte Carlo simulations, which will indicate how much confidence one can put in the LPDM output used during flight planning. Nonetheless, the strong correlation between receptor averaged and domain BLB fluxes indicate that the current LPDM output did a decent job at partitioning the measurements.

Mesoscale models provide an effective tool to study local circulations in complex terrain. When combined with meteorological observations, it provides us a way to evaluate whether the model is able to simulate these complex flows (*De Wekker et al.*, 2009). Here we compared model output with observations from the Denver International Airport 12Z sounding and NWR on 21 June 2007. Observations from the 12Z sounding compare well with model output. There are, however, a few discrepancies. The biggest differences are in lower level (below 6 km) wind speeds and dew point temperatures and upper level (above 14 km) wind directions. For this study we were concerned with the way the model simulated boundary layer processes which affect the spatial distribution and transportation of atmospheric tracers in the lower troposphere. In the boundary layer, wind speeds differ by as much as 5 m s^{-1}. This difference, over an hour, translates to an 18 km spread in the spatial distribution of the released particles. Modeled dew point temperatures in the boundary layer are also 20° C cooler. Cooler dew point temperatures affect the water vapor mixing ratio and the 3-D transportation of atmospheric tracers. Yet, the strong similarity between model output and the 12Z sounding indicate that the current simulation is able to capture most of the synoptic flow pattern on this day.

However, observations from NWR show a different story. NWR was used to examine whether the current simulation was able to capture complex local flows at a mountain top location. This study focused on the way the observations and RAMS model output compared with one another from 1500 UTC onward. From this time-step forward, there are large differences in water vapor mixing ratio and wind direction. These difference play a crucial role in the spatial distribution of atmospheric tracers in complex terrain. Difference in wind direction will cause the particles to be transported in the wrong direc-

tion while difference in water vapor mixing ratio affects how the particles are transported in all dimensions. These differences indicate the inability of the current model run to simulate complex circulations in mountainous terrain. Therefore, further runs need to be performed in order to obtain the optimal model parameters that are consistent with observations and able to simulate local flows around NWR and in complex terrain.

Although there were large differences between observations and model output at NWR, the strong similarity with the 12Z sounding from the Denver International Airport gives confidence that the current simulation is able to capture the general synoptic flow pattern. With this added confidence, a LPDM was used to simulate the dispersion of particles around the domain. Despite the differences between observations and model output at NWR, results from HYPACT suggests that the measurement strategy used during ACME07 did a good job at chasing air masses due to the similarities between the particle distribution and the flight profile. The afternoon downwind flight profile flew directly between the particles. This hints that the afternoon flight, on this day, could have been postponed by a few hours in order to obtain a more representative sampling. It also indicates that the flight profile could have been shifted towards the west. However, if this was done, it would have nullified parcel trajectory flux calculations because the measurement strategy was designed to sample receptor source locations during the morning upwind flights and around the receptor during the afternoon downwind flights. The parcel trajectory flux approach, combined with the use of multiple parallel profiles, was designed to account for flux variations caused by complex terrain and large shear. Nevertheless, the approach taken during ACME07 to sample the spatial distribution and concentration of regional CO_2 did an excellent job in chasing air mass as it moved through the domain and increases the reliability of the BLB method to compute regional surface carbon fluxes. Based upon the findings in this thesis and those obtained from COBRA (*Gerbig et al.*, 2003*a,b*; *Lin et al.*, 2004, 2006, 2007), CERES (*Dolman et al.*, 2006), and ACME07 (*Sun et al.*, 2010) further multi-scale and multidisciplinary studies need to be conducted and addressed in order to further quantify the carbon sequestration possibilities of North America.

5   Conclusion

Analysis of the airborne measurements from ACME07 enabled the computation of regional carbon fluxes over the Central Rocky Mountains (Figure 3). Airborne flux estimates were combined with estimates from NWR and CarbonTracker in order to gain a better understanding of the seasonal pattern and magnitude of carbon uptake in the Central Rocky Mountains. Comparison among the three estimates yielded similar magnitudes and patterns but distinct differences in the timing of peak uptake and ecosystem drought stress. Receptor averaged and total domain BLB fluxes indicate that this region is likely an important carbon sink for the Western United States, -7.54 μmol m^{-2} s^{-1}. The carbon sequestration potential of the Central Rocky Mountains is greater than a shrub wetland but significantly less than an old growth forest. However, conducting airborne campaigns are expensive and time consuming. Therefore, understanding how the BLB fluxes from ACME07 compare with other estimates that are readily available will allow one to make assumptions about regional carbon fluxes and its impact on the surrounding ecosystems.

The BLB method used to compute the airborne carbon fluxes required accurate estimates of the maximum boundary layer height. Therefore, various boundary layer height estimates were obtained and used to see how changing this height affected the flux calculated. Despite the differences between the maximum boundary layer heights, there were strong similarities among the flux estimates computed with them. This was expected due to the lack of correlation between the growth of the boundary layer and the spatial distribution of CO_2. Regardless of the height used in the computation, as long as it exceeded the height of the mountaintops, it only has a small effect of the surface fluxes calculated. As such, changes in the maximum boundary layer height, which had a combined uncertainty of 25%, lead to a 26% spread in the BLB flux.

Computation of surface fluxes using the BLB method also relies on our ability to track and chase air masses as it moves across the domain. To test whether the experiment was successful in doing this, a mesoscale model was run in tandem with a LPDM. Use of a mesoscale model, when combined with observations, enables one to study the local

flow patterns associated with complex terrain. When combined with a LPDM, the role of vertical mixing of passive tracers can be identified. Here, the LPDM was used to determine whether the measurement strategy used during ACME07 was able to chase and sample the correct air mass. Analysis of the spatial distribution of the particles released from five upwind source locations reveals that the measurement strategy was able to chase air masses across the domain. However, timing of the flight seem to off by an hour or two.

The results presented here only give a small picture of regional carbon exchange in the Central Rocky Mountains. There are several more experiments and projects that need to be performed in order to obtain a more complete picture. With regards to these results, further RAMS simulations need to be performed in order to correctly simulate the complex local circulations associated with the Rocky Mountains. With these simulations, HYPACT can be used to release particles, in the forward trajectory mode, along the morning upwind flight profile to determine its influence and footprint on the afternoon downwind flight. The same can be done in the back-trajectory mode in order to identify precise upwind source locations for receptor based flux calculations. With the uncertainties in BLB fluxes narrowed down, the airborne measurements can be assimilated into an ecosystem based model for comparison. This would allow for the measurements to be analyzed using a different bottom-up approach. The airborne measurements can also be assimilated into a regional inverse model, in a top-down approach, to further narrow down the pattern of regional carbon exchange in the Central Rocky Mountain and assess its impact on the surrounding climate and ecosystems.

References

American Meteorological Society, *Glossary of Meteorology, Second Edition*, 850 pp., Allen Press, 2000.

Betts, A.K., R.L. Desjardins, and J.I. MacPherson, Budget Analysis of the Boundary Layer Grid Flights During FIFE 1987, *J. Geophys. Res.*, *97*(D17), 18533–18546, 1992.

Cotton, W.R., R.A. Pielke, R.L. Walko, G.E. Liston, C.J. Tremback, H. Jiang, R.L. McAnelly, J.Y. Harrington, M.E. Nicholls, G.G. Carrio, and J.P. McFadden, RAMS 2001: Current status and future directions, *Meteor. Atmos. Phys.*, *82*, 5–29, 2003.

De Wekker, S.F.J., A. Ameen, G. Song, B.B. Stephens, A.G. Hallar, and I.B. McCubbin, A Preliminary Investigation of Boundary Layer Effects on Daytime Atmospheric CO_2 Concentrations at a Mountaintop Location in the Rocky Mountains, *Acta Geophysica*, *57*(4), 904–922, 2009.

Desai, A.R., A. Noormets adn P.V. Bolstand, J. Chen, B.D. Cook, K.J. Davis, E.S. Euskirchen, C. Gough, J.G. Martin, D.M. Ricciuto, H.P. Schmid, J. Tang, and W. Wang, Influence of vegetation and seasonal forcing on carbon dioxide fluxes across the Upper Midwest, USA: Implications for regional scaling, *Agricultural and Forest Meteorology*, *148*(2), 288–308, 2008.

Dolman, A.J., J. Noilhan, P. Durand, C. Sarrat, A. Burt, B. Piguet, A. Butet, N. Jarosz, Y. Burnet, D. Loustau, E. Lamaud, L. Tolk, R. Ronda, F. Miglietta, B. Fioli, V. Magliulo, M. Esposito, C. Gerbig, S. Körner, P. Glademard, M. Ramonte, P. Ciais, B. Neininger, R.W.A. Hutjes, J.A. Elbers, R. Macatangay, O. Schrems, F. Pérez-Landa, M.J. Sanz, Y. Scholz, G. Facon, E. Ceschia, and P. Beziat, The CarboEurope Regional Experiment Strategy, *Bull. Amer. Met. Soc.*, *87*(10), 1367–1379, 2006.

Garratt, J.R., The Internal Boundary Layer - A Review, *Bound.-Layer Meteo.*, *50*, 171–203, 1990.

Gerbig, C., J.C. Lin, S.C. Wofsy, B.C. Daube, A.E. Andrews, B.B. Stephens, P.S. Bakwin, and C. A. Grainger, Toward constraining regional-scale fluxes of CO_2 with atmospheric observations over a continent: 1. Observed spatial variability from airborne platforms, *J. Geophys. Res.*, *108*(D24), 4756, 2003*a*.

Gerbig, C., J.C. Lin, S.C. Wofsy, B.C. Daube, A.E. Andrews, B.B. Stephens, P.S. Bakwin, and C. A. Grainger, Toward constraining regional-scale fluxes of CO_2 with atmospheric observations over a continent: 2. Analysis of COBRA data using a receptor-oriented framework, *J. Geophys. Res.*, *108*(D24), 4757, 2003*b*.

Gerbig, C., J.C. Lin, J.W. Munger, and S.C. Wofsy, What can tracer observations in the continental boundary layer tell us about surface-atmosphere fluxes?, *Atmos. Chem. Phys.*, *6*, 539–554, 2006.

Gerbig, C., A.J. Dolman, and M. Heimann, On observational and modelling strategies targeted at regional carbon exchange over continents, *Biogeoscience Discuss.*, *6*, 1317–1343, 2009.

Goulden, M.L., J.W. Munger, S. Fan, B.C. Daube, and S.C. Wofsy, Measurements of Carbon Sequestration by long-term eddy covariance: methods and a critical evaluation of accuracy, *Global Change Biol.*, *2*, 169–182, 1996.

Gourdji, S., A.I. Hirsch, K. Muellerand A.E. Andrews, and A.M. Michalak, Regional-scale geostatistical inverse modeling of North American CO_2 fluxes: A synthetic data study, *Atmos. Chem. Phys. Discuss.*, *9*, 22407–22458, 2009.

Grimsdell, A.W., and W.M. Angevine, Convective Boundary Layer Height Measurement with Wind Profilers and Comparison to Cloud Base, *J. Atmos. Oceanic Technol.*, *15*, 1331–1338, 1998.

Gurney, K.R., R.M. Law, A.S. Denning, P.J. Rayner, D. Baker, P. Bousquet, L. Bruhwiler, Y. Chen, P. Ciais, S. Fan, I.Y. Fung, M. Gloor, M. Heimann, K. Higuchi, J. John, T. Maki, S. Maksyutov, K. Masarie, P. Peylin, M. Prather, B.C. Pak, J. Randerson, J. Sarmiento, S. Taguchi, T. Takahashi, and C. Yuen, Towards Robust Regional Estimates of CO_2 Sources and Sinks using Atmospheric Transport Models, *Nature*, *415*, 626–630, 2002.

Holzworth, G.C., Estimates of Mean Maximum Mixing Depth in the Contiguous United States, *Mon. Wea. Rev.*, *92*(5), 235–242, 1964.

Janjić, Z., The step-mountain coordinate: Physical Package, *Mon. Wea. Rev.*, *118*, 1429–1443, 1990.

Kalthoff, N., H.-J. Binder, M. Kossmann, R. Vögtlin, U. Corsmeier, F. Fiedler, and H. Schlager, Temporal Evolution and Spatial Variation of the Boundary Layer over Complex Terrain, *Atmos. Environ.*, *32*(7), 1179–1194, 1998.

Keane, R.E., K.C. Ryan, T.T. Veblen, C.D Allen, J.A. Logan, and B. Hawkes, The Cascading Effects of Fire Exclusion in Rocky Mountain Ecosystems, in *Rocky Mountain Futures: An Ecological Perspective*, edited by J.S. Baron, pp. 133–152, Island Press, 2002.

Keeling, C.D., R.B. Bacastow, A.E. Bainbridge, C.A. Ekdahl, P.R. Guenther, and L.S. Waterman, Atmospheric carbon dioxide variations at Mauna Loa Observatory, Hawaii, *Tellus*, *28*, 538–551, 1976.

Krol, M., S. Houweling, B. Bergman, M. van Den Broek, A. Segers, P. van Velthoven, W. Peters, F. Dentener, and P. Bergamaschi, The two-way nested global chemistry-transport zoom model TM5: algorithm and applications, *Atmos. Chem. Phys.*, *5*(2), 417–432, 2005.

Kurz, W.A., C.C. Dymond, G. Stinson, G.J. Rampley, E.T. Neilson, A.L. Carroll, T. Ebata, and L. Safranyik, Mountain pine beetle and forest carbon feedback to climate change, *Nature*, *452*, 987–990, 2008.

Lin, J.C., C. Gerbig, S.C. Wofsy, A.E. Andrews, B.C. Daube, K.J. Davis, and C.A. Grainger, A near-field tool for simulating the upstream influence of atmospheric observations: The Stochastic Time-Inverted Lagrangian Transport (STILT) model, *J. Geophys. Res.*, *108*(D16), 4493, 2003.

Lin, J.C., C. Gerbig, S.C. Wofsy, A.E. Andrews, B.C. Daube, C.A. Grainger, B.B. Stephens, P.S. Bakwin, and D.Y. Hollinger, Measuring fluxes of trace gases at regional scales by Lagrangian observations: Application to the CO_2 Budget and Rectification Airborne (COBRA) study, *J. Geophys. Res.*, *109*(D15304), 2004.

Lin, J.C., C. Gerbig, S.C. Wofsy, B.C. Daube, D.M. Matross, V.Y. Chow, E. Gottlieb, A.E. Andrews, M. Pathmathevan, and J.W. Munger, What have we learned from intensive atmospheric sampling field programmes of CO_2, *Tellus*, *58B*, 331–343, 2006.

Lin, J.C., C. Gerbig, S.C. Wofsy, V.Y. Chow, E. Gottlieb, B.C. Daube, and D.M. Matross, Designing Lagrangian experiments to measure regional-scale trace gas fluxes, *J. Geophys. Res.*, *112*, D13312, 2007.

Lloyd, J., O. Kolle, H. Fritsch, S.R. de Freitas, M.A.F. Silva Dias, P. Artaxo, A.D. Nobre, A.C. de Araújo, B. Kruijt, L. Sogavheva, G. Fisch, A. Thielmann, U. Kuhn, and M.O. Andreae, An airborne regional carbon balance for Central Amazonia, *Biogeosciences*, *4*, 759–768, 2007.

Mesinger, F., G. DiMego, E. Kalnay, K. Mitchell, P.C. Shafran, W. Ebisuzaki, D. Jović, J. Woollen, E. Rogers, E.H. Berbery, M.B. Ek, Y. Fan, R. Grumbine, W. Higgins, H. Li, Y. Lin, G. Manikin, D. Parrish, and W. Shi, North American Regional Reanalysis, *Bull. Amer. Met. Soc.*, *87*(3), 343–360, 2006.

Monson, R.K., A.A. Turnipseed, J.P. Sparks, P.C. Harley, L.E. Scott-Denton, K. Sparks, and T.E. Huxman, Carbon sequestration in a high-elevation, subalpine forest, *Global Change Biol.*, *8*, 459–478, 2002.

Peters, W., A.R. Jacobson, C. Sweeney, A.E. Andrews, T.J. Conway, K. Masarie, J.B. Miller, L.M.P. Bruhwiler, G. Pétron, A.I. Hirsch, D.E.J. Worthy, G.R. van der Werf, J.T. Randerson, P.O. Wennberg, M.C. Krol, and P.P. Tans, An atmospheric perspective on North American carbon dioxide exchange: CarbonTracker, *Proceedings of the National Academy of Science*, *104*(48), 18925–18930, 2007.

Pielke, R.A., W.R. Cotton, R.L. Walko, C.J. Tremback, W.A. Lyons, L.D. Grasso, M.E. Nichollos, M.D. Moran, D.A. Wesley, T.J. Lee, and J.H. Copeland, A comprehensive meteorological modeling system - RAMS, *Meteor. Atmos. Phys.*, *49*, 69–91, 1992.

Pleim, J.E., and A. Xiu, Development and testing of a surface flux and planetary boundary layer model for application in mesoscale models, *J. Appl. Meteor.*, *34*, 16–32, 1995.

Raffa, K.F., B.H. Aukema, B.J. Bentz, A.L. Carroll, J.A. Hicke, M.G. Turner, and W.H. Romme, Cross-scale Drivers of Natural Disturbances Prone to Anthropogenic Amplification: The Dynamics of Bark Beetle Eruptions, *BioScience*, *58*(6), 501–517, 2008.

Raupach, M.R., O.T. Denmead, and F.X. Dunin, Challenges in Linking Atmospheric CO_2 Concentrations to Fluxes at Local and Regional Scales, *Aust. J. Bot.*, *40*, 697–716, 1992.

Sarrat, C., J. Noilhan, P. Lacarrére, E. Ceschia, P. Ciais, A. Dolman, J. A. Elbers, C. Gerbig, B. Gioli, T. Lauvaux, F. Miglietta, B. Neininger, M. Ramonet, O. Vellinga, and J.-M. Bonnefond, Mesoscale modelling of the CO_2 interactions between the surface and the atmosphere applied to the April 2007 CERES field experiment, *Biogeosciences*, *6*, 633–646, 2009.

Schimel, D., T.G.F. Kittel, S. Running, R. Monson, A. Turnipseed, and D. Anderson, Carbon sequestration studied in western U.S. mountains, *EOS, Trans. Amer. Geophys. Union*, *83*, 445–449, 2002.

Stephens, B.B., A. Watt, and G Maclean, An Autonomous Inexpensive Robust CO_2 Analyzer (AIRCOA). 13th WMO/IAEA Meeting of Experts on Carbon Dioxide Concentration and Related Tracers Measurements Techniques, *WMO TD*, *1359*, 95–99, 2006.

Stohl, A., M. Hittenberger, and G. Wotawa, Validation of the Lagrangian particle dispersion model FLEXPART against large scale tracer experiments, *Atmos. Environ.*, *32*, 4245–4264, 1998.

Stohl, A., C. Forster, A. Frank, P. Seibert, and G. Wotawa, Technical Note : The Lagrangian particle dispersion model FLEXPART version 6.2, *Atmos. Chem. Phys.*, *5*, 2461–2474, 2005.

Stull, R.B., *An Introduction to Boundary Layer Meteorology*, 670 pp., Springer, 1988.

Sulman, B.N., A.R. Desai, B.D. Cook, N. Saliendra, and D.S. Mackay, Contrasting carbon dioxide fluxes between a drying shrub wetland in Northern Wisconsin, USA, and nearby forests, *Biogeosciences*, *6*, 1115–1126, 2009.

Sun, J., S.P. Oncley, S.P. Burns, B.B. Stephens, D.H. Lenschow, T. Campos, A.S. Watt, R.K. Monson, D.J.P. Moore, J. Hu, M. Tschudi, D.S. Schimel, S. Aulenbach, W.J. Sacks, S.F.J. DeWekker, C. Lai, B. Lamb, E. Allwine, T. Coons, D. Ojima, P.Z. Ellsworth, L.S.L. Sternberg, S. Zhong, C. Clements, and D.E. Anderson, A Multiscale and Multidisciplinary Investigation Of Ecosystem-Atmosphere CO_2 Exchange Over the Rocky Mountains of Colorado, *Bull. Amer. Met. Soc.*, *91*(2), 209–230, 2010.

Walko, R.L., L.E. Band, J. Baron, T.G.F. Kittel, R. Lammers, T.J. Lee, D.S. Ojima, R.A. Pielke, C. Taylor, C. Tague, C.J. Tremback, and P.L. Vidale, Coupled atmosphere-biophysics-hydrology models for environmental modeling, *J. Appl. Meteor.*, *39*, 931–944, 2000.

Walko, R.L., C.J. Tremback, and M.J. Bell, HYPACT. HYbrid Particle And Concentration Transport Model, Version 1.5. User's Guide. 35 pp., Website, 2007, http://www.atmet.com/index.shtml.

Wallace, J.M., and P.V. Hobbs, *Atmospheric Science: An Introductory Survey*, 467 pp., Academic Press, 1977.

Whiteman, C.D., *Mountain Meteorology: Fundamentals and Applications*, 355 pp., Oxford University Press, 2000.
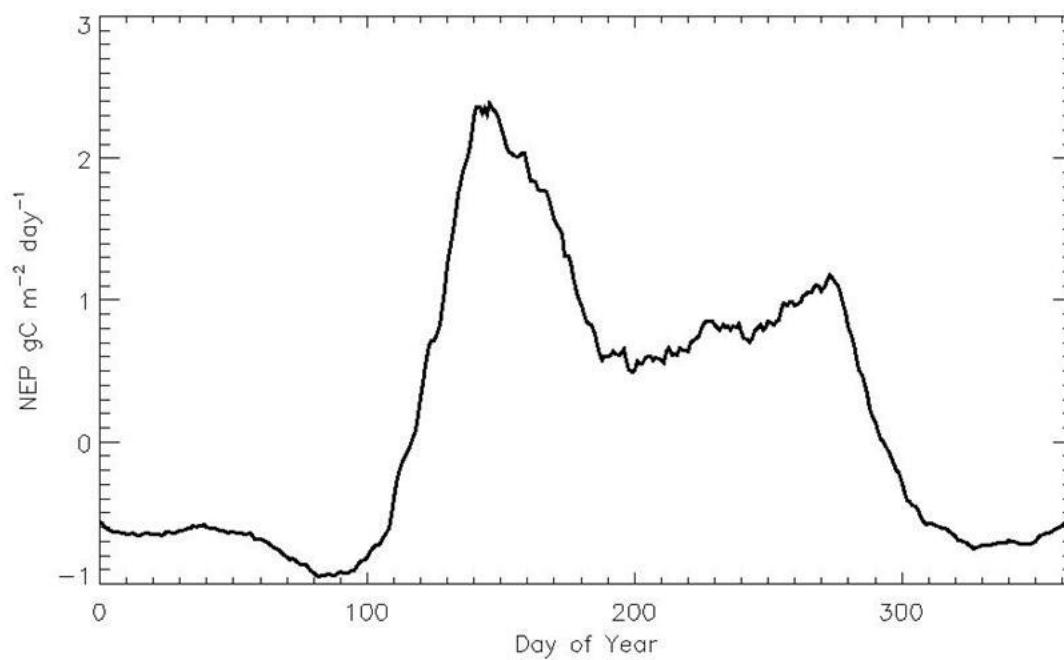
Figure 1: 10-year averaged net ecosystem productivity (NEP), in g C m^{-2} day^{-1}, from the Niwot Ridge (NWR) Ameriflux Site. NEP is smoothed with a 10-day running mean. Peak uptake of carbon occurs in the early summer, followed by a decrease in uptake due to summer drought stress. Uptake increases, with a secondary maximum, with the onset of the North American Summer Monsoon. Figure is courtesy of R. Monson, CU - Boulder.
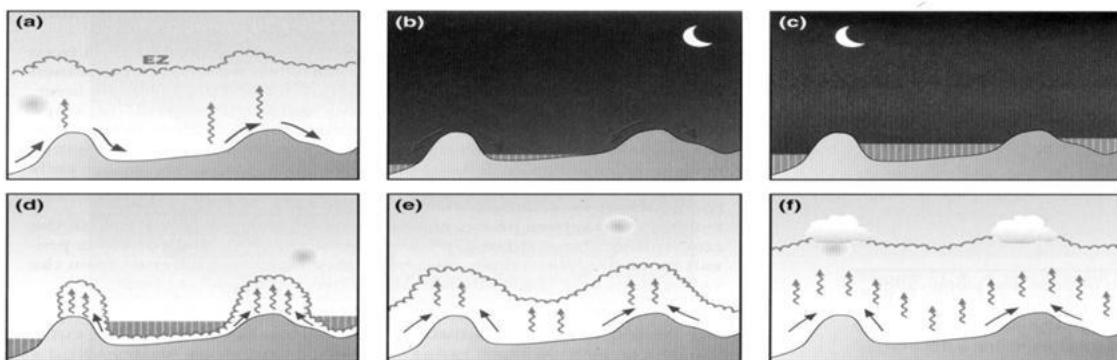
Figure 2: Structure of the atmospheric boundary layer in mountainous regions (*White-man*, 2000). Shown are the evening transition phase (a and b), the nighttime phase (c), morning transition phase (d and e), and afternoon phase (f).
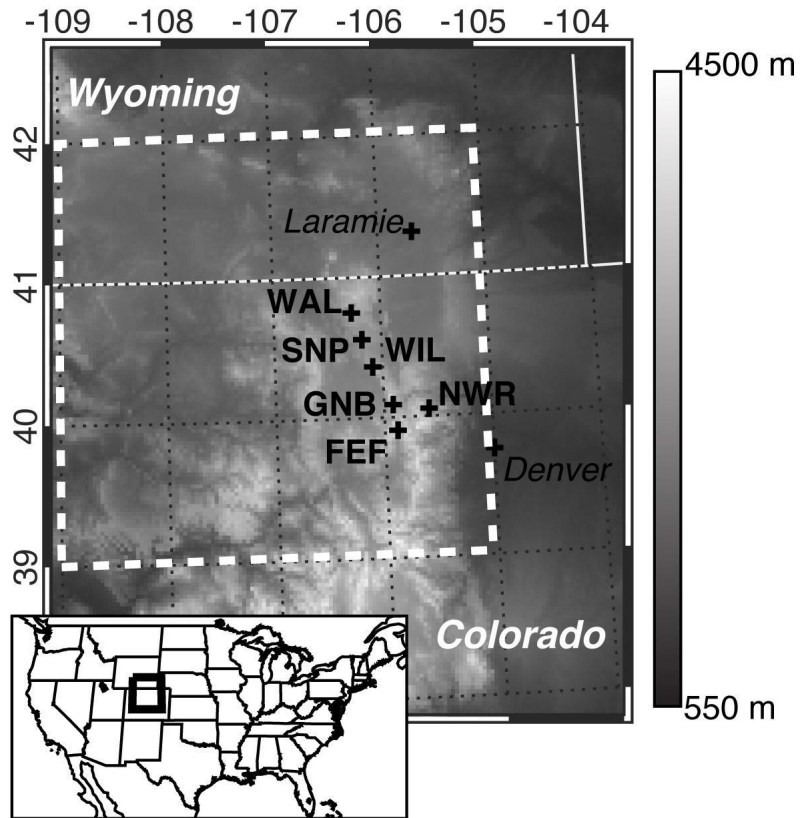
Figure 3: Topographic map of the ACME07 domain. Shown for spatial reference are Laramie, WY, USA (takeoff point) and Denver, CO, USA. Also shown are the receptor locations (Table 2) for the afternoon downwind flights and NWR. In general, higher elevations are dominated by forest ecosystems. Figure is courtesy of A. Desai, UW - Madison.
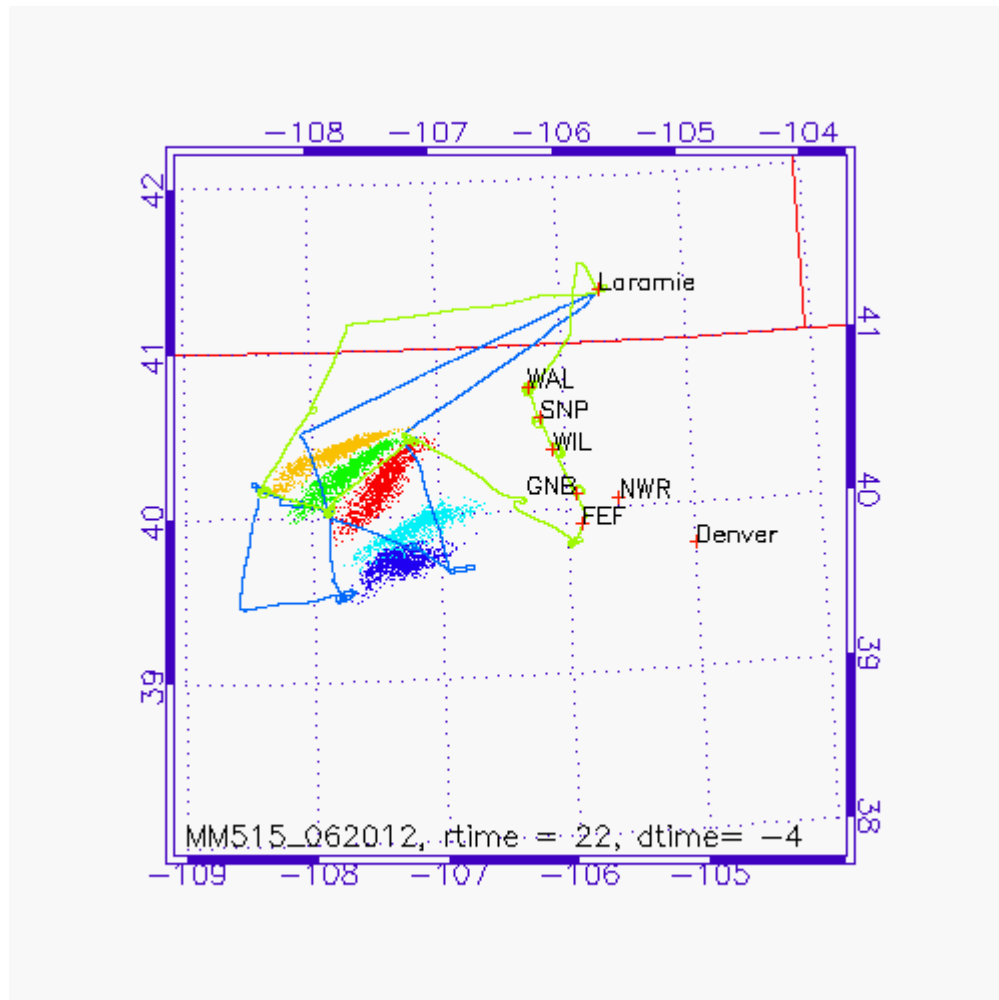
Figure 4: Particle dispersion map used for flight planning purposes. Shown for spatial reference are Laramie, WY, USA (takeoff point) and Denver, CO, USA. Also shown are the five downwind receptors (Table 2), NWR, and the morning upwind (blue) and afternoon downwind (green) flight profiles. Particle dispersion is computed with STILT using the MM5 15 km model forecast, valid on 20 June 2007 at 1200 UTC. Particles were released from the receptors, in the back-trajectory mode, at 2200 UTC. Spatial distribution of the released particles is shown at 1800 UTC. Notice the multiple parallel profiles flown during the morning upwind flight in order to account for flux variations caused by non-homogeneous terrain and large vertical shear. For reference, synoptic winds are from the southwest.
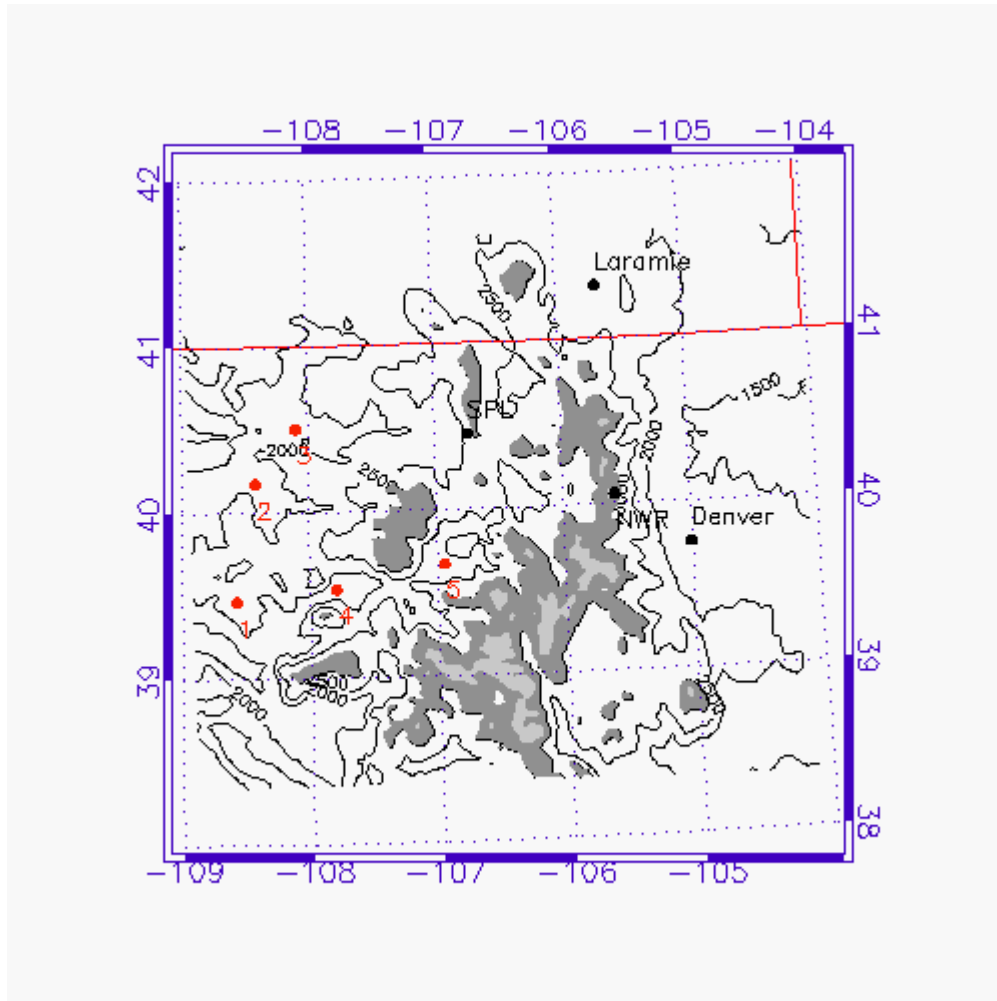
Figure 5: Topographic map of the area covered by the RAMS and HYPACT simulations. Contours are drawn every 500 m. Dark gray and light gray shading represent elevations between 3000 and 3500 m MSL and above 3500 m MSL, respectively. Shown for spatial reference are the locations of Laramie, WY, USA (takeoff point), Storm Peak Laboratory (SPL), NWR and Denver, CO, USA. Also shown are the locations of the five sources (red) used in the HYPACT simulation. The source number corresponds to those in Table 4.
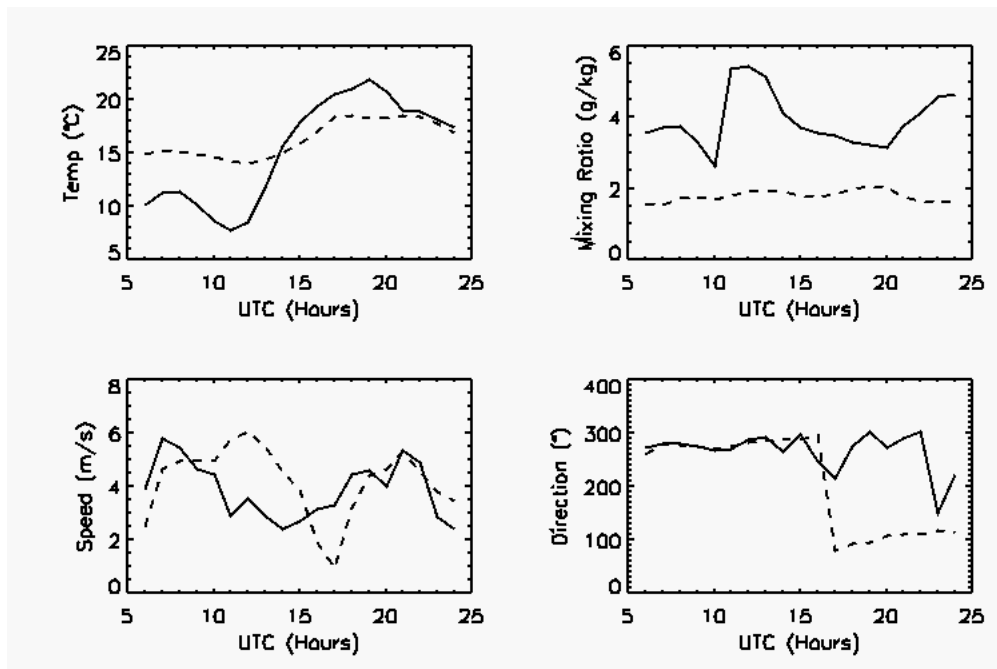
Figure 6: Observations (solid line) and model output (dashed line) from NWR. Shown are temperature (top left), water vapor mixing ratio (top right), and wind speed (bottom left) and direction (bottom right). Mismatch between observations and model output indicate that the current simulation is not able to resolve some of the complex local flows around NWR.
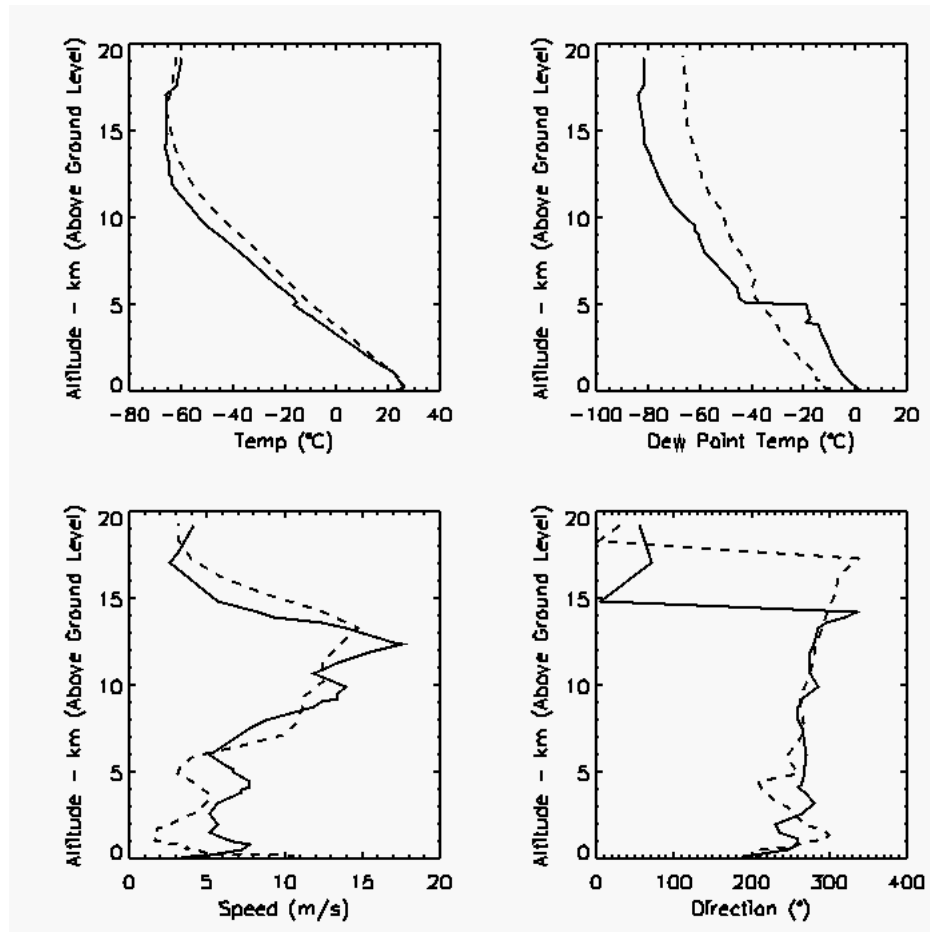
Figure 7: Observations (solid line) and model output (dashed line) from the 21 June 2007, 12Z sounding at the Denver International Airport, USA. Shown are temperature (top left), dew point temperature (top right), and wind speed (bottom left) and direction (bottom right). Strong correlations throughout the profile indicate that the current simulation is able to model the general synoptic pattern.
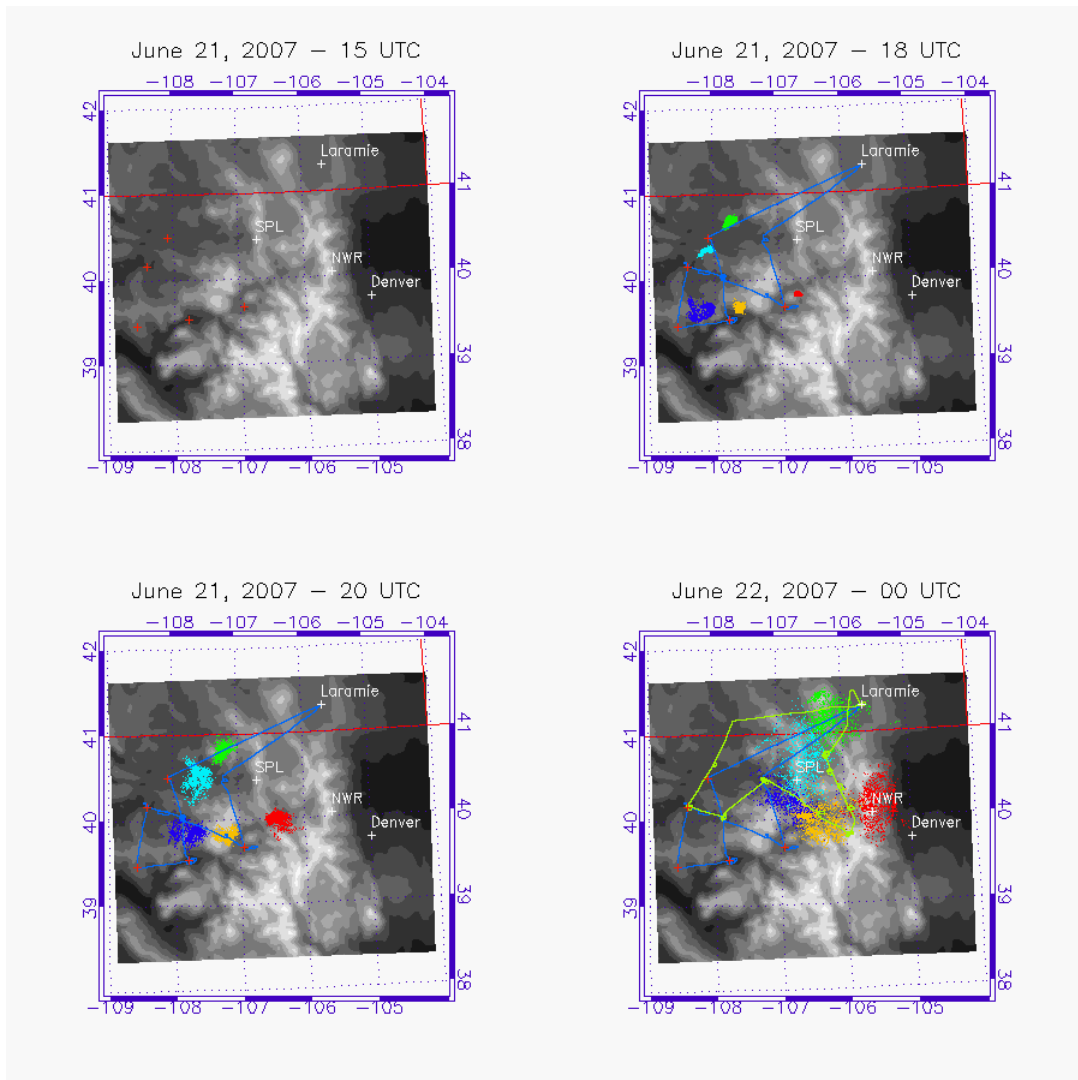
Figure 8: Particle dispersion results from HYPACT on 21 June 2007. Particles were released from five upwind sources (red crosses) at 1500 UTC (top left), shortly after takeoff of the morning upwind flight. Also shown are the spatial distribution of the particles shortly before touchdown of the morning flight (blue line) at 1800 UTC (top right), 30 minutes before takeoff of the afternoon downwind flight at 2000 UTC (bottom left) and shortly after touchdown of the afternoon flight (green line) at 0000 UTC, 22 June 2007 (bottom right). For spatial reference, the locations of Laramie, WY, USA (takeoff point), SPL, NWR and Denver, CO, USA are displayed with model topography in the background (light colors represent higher elevations).
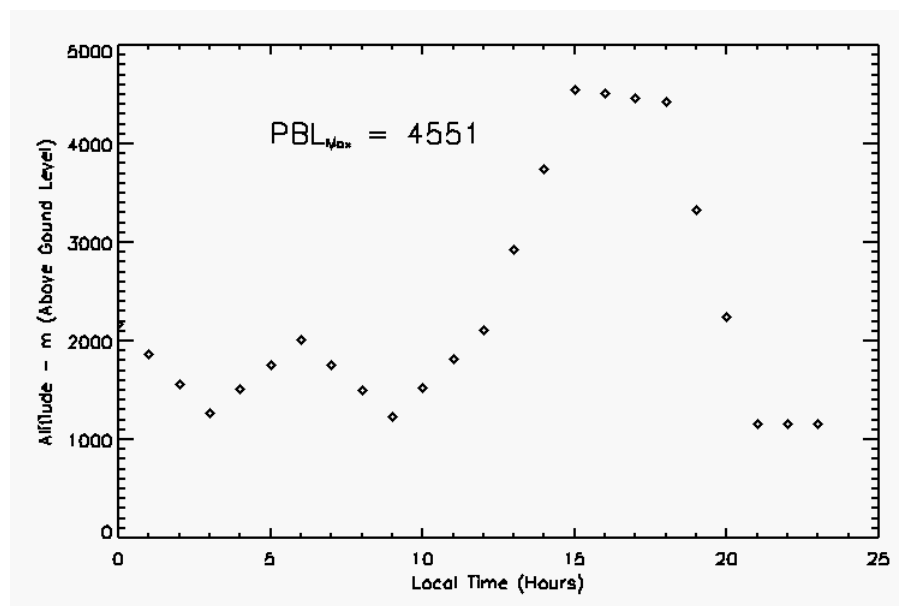
Figure 9: Evolution of the boundary layer on 21 June 2007 from NARR. Three-hourly surface meteorology was interpolated to hourly resolution. Time is in Local Time (MST). Maximum boundary layer height on this day was 4551 m above ground level.
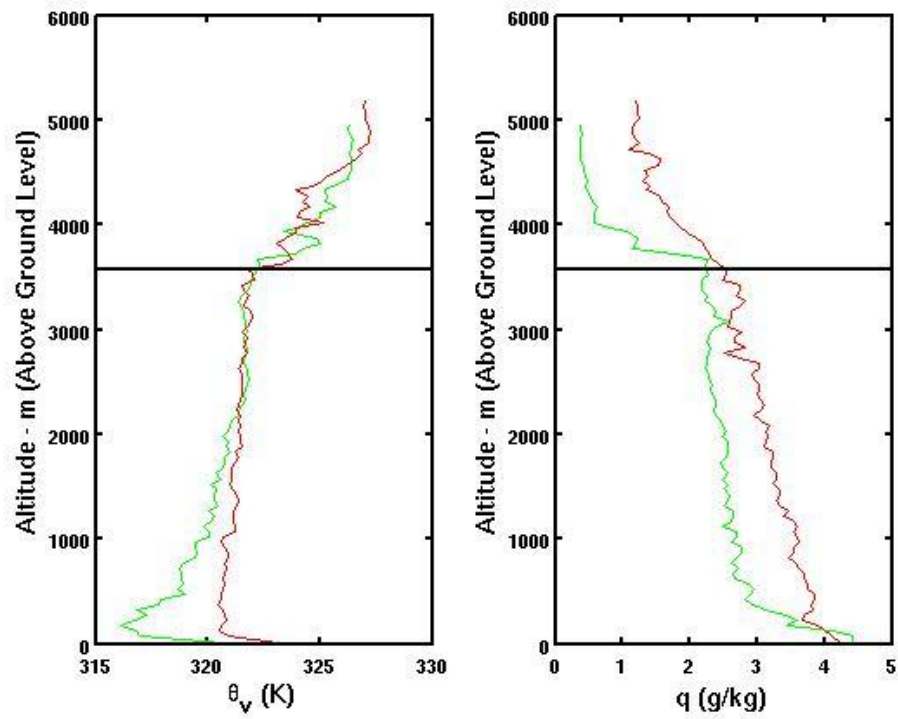
Figure 10: Vertical profiles of θ_v and q on 21 June 2007 from the morning upwind (green), 0853-1001 LT, and afternoon downwind (red), 1424-1755 LT, flights. θ_v and q are averaged into 50 m vertical bins. Horizontal line in both profiles represent the maximum boundary layer height, 3574 m.
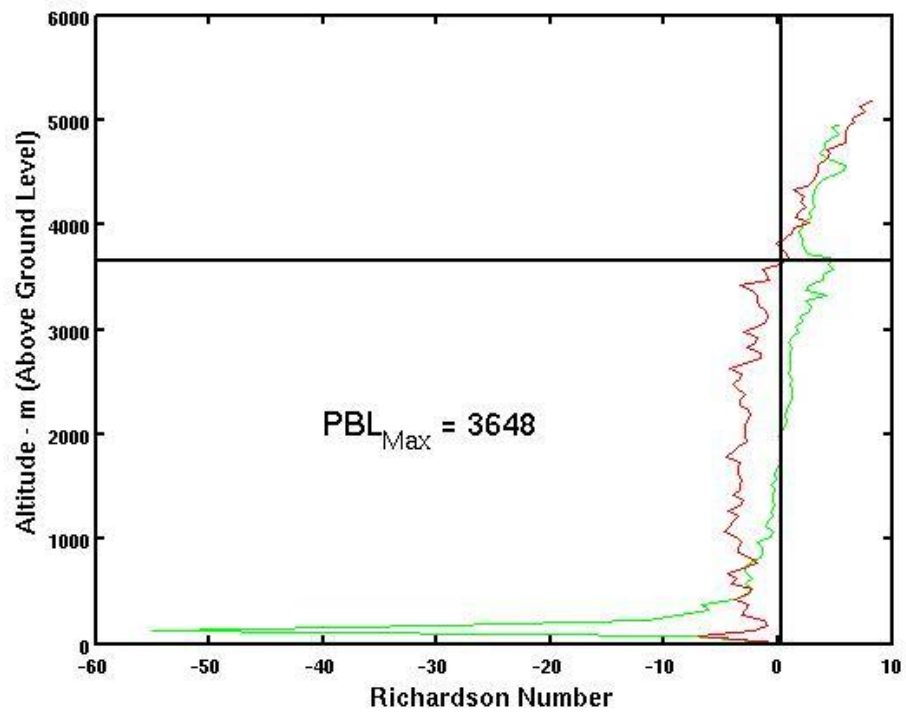
Figure 11: Vertical profile of Ri_B on 21 June 2007 from the morning upwind (green) and afternoon downwind (red) flights. Ri_B is averaged into 50 m vertical bins. Ri_c was chosen to be 0.25 (vertical line). Horizontal line represent the maximum boundary layer height, 3648 m.
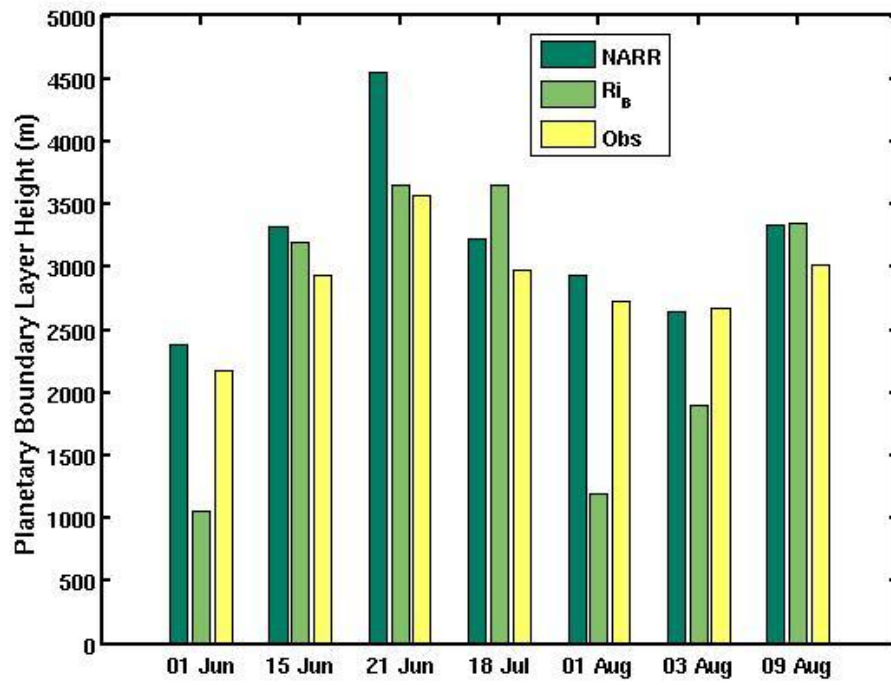
Figure 12: Bar plot of NARR (green), Ri_B (light green), and observed (yellow) boundary layer heights from the seven flight days analyzed (Table 1). Observed heights refer to those obtained via the parcel method.
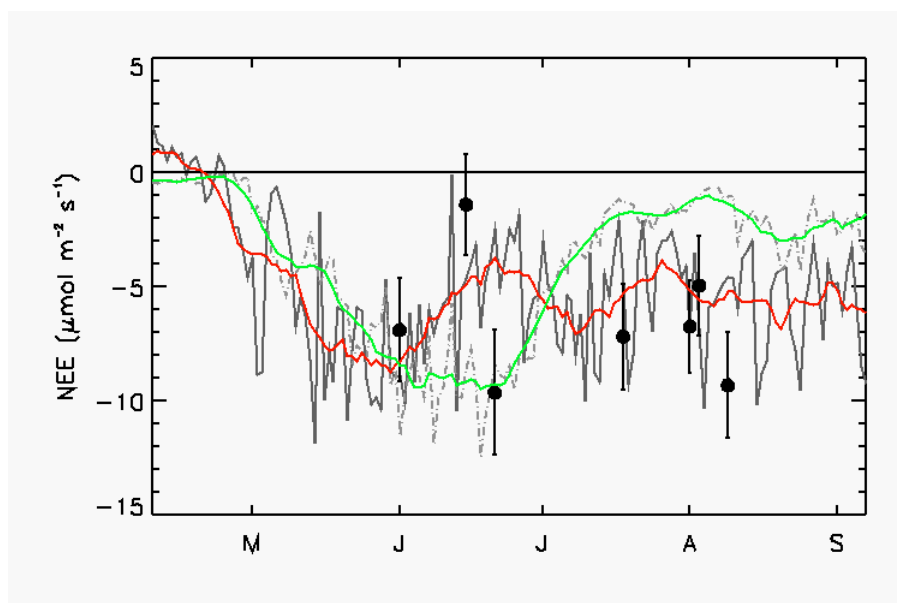
Figure 13: Time series of regional fluxes, in μmol m^{-2} s^{-1}, from BLB calculated using the observed boundary layer heights (circle), daytime average from NWR (solid line), and daytime and domain average from CarbonTracker (dot-dashed line). Errors for BLB fluxes are based upon the uncertainty in CO_2 concentrations and boundary layer height. Also shown are the 10-day running average flux from NWR (red line) and CarbonTracker (green line). Observed heights refer to those obtained via the parcel method.
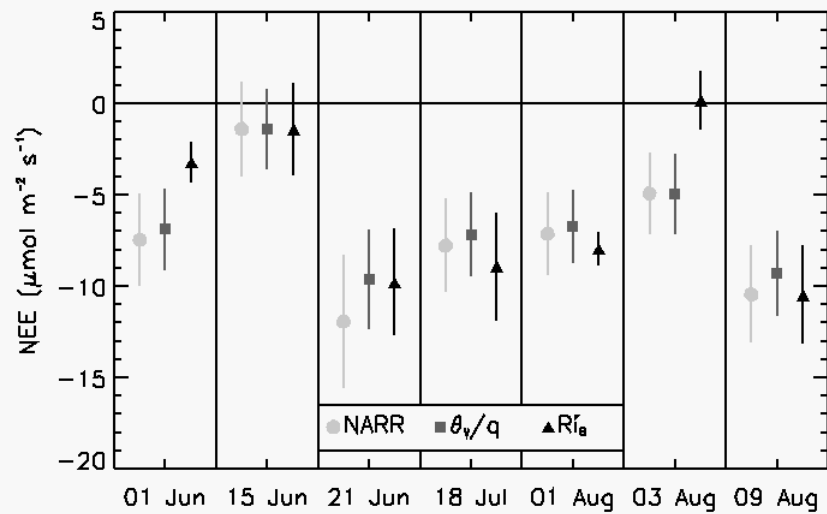
Figure 14: BLB fluxes, in μmol m^{-2} s^{-1}, calculated using the various estimates of boundary layer heights. Shown are BLB fluxes using NARR boundary layer heights (circle), the boundary layer heights from θ_v/q (square), and from the bulk Richardson number approach (triangle). Errors for BLB fluxes are based upon the uncertainty in CO_2 concentrations and boundary layer height. Case numbers refer to those from Table 1.

Figure 15: Comparison between BLB fluxes, in μmol m^{-2} s^{-1}, from the total domain, computed using the parcel method boundary layer heights, and parcel trajectory average. Errors for BLB fluxes are based upon the uncertainty in CO_2 concentrations and boundary layer height. Correlation between the two fluxes is 0.83 with a slope of 0.66. Numbers refer to those from Table 1.
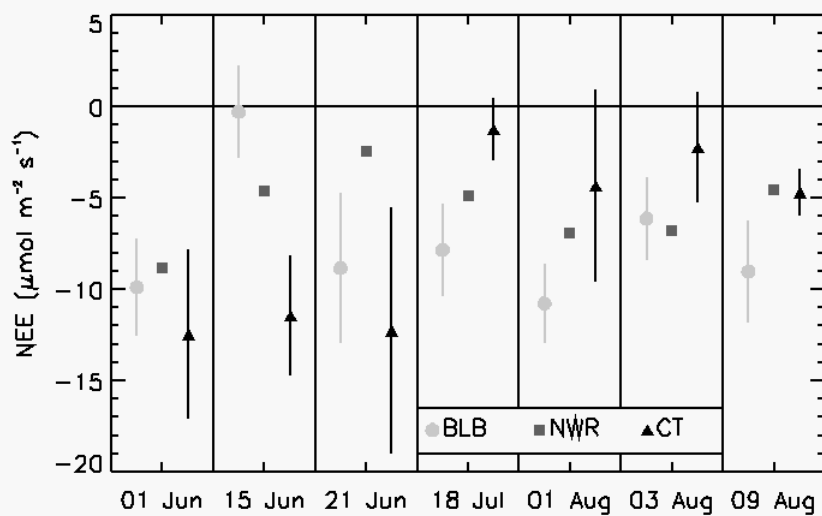
Figure 16: Regional fluxes, in μmol m^{-2} s^{-1}. Shown are the receptor average BLB flux (circle), daytime average NWR flux (square), and CarbonTracker fluxes (triangle), computed over the footprint of the flights (Table 3). Errors for BLB fluxes are based upon the uncertainty in $CO_2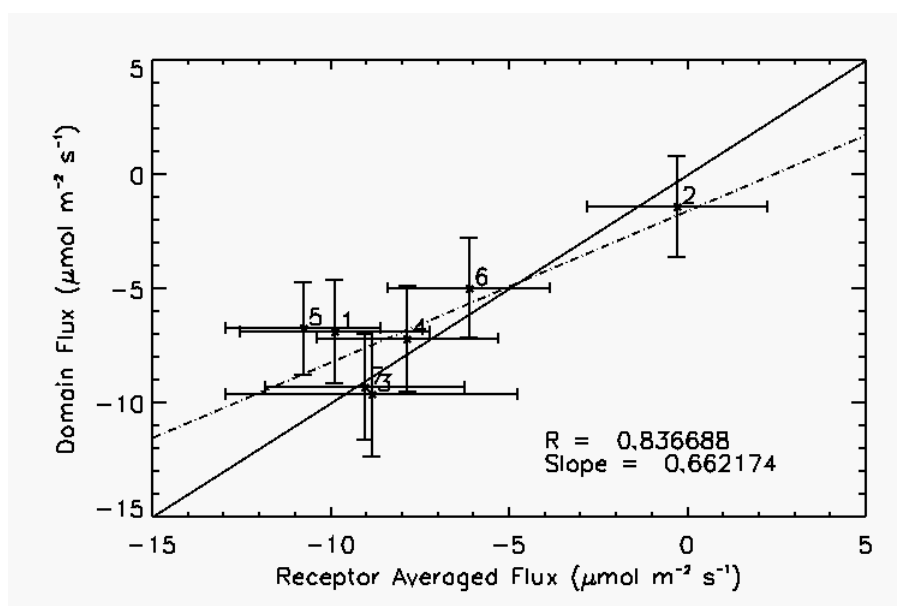$ concentrations and boundary layer height. Errors from CarbonTracker represent the 1-σ spatial variability. Case numbers refer to those from Table 1.

Table 1: Flight times (takeoff to touchdown) for the morning upwind and afternoon downwind paired flights used in this study. Local time is UTC - 6 hours.

Case	Date	Upwind (UTC)	Downwind (UTC)
1	1 Jun	1353-1710	1856-2028
2	15 Jun	1420-1740	2021-2310
3	21 Jun	1453-1801	2024-2355
4	18 Jul	1500-1740	2023-2319
5	1 Aug	1331-1720	2007-2221
6	3 Aug	1406-1758	2010-2215
7	9 Aug	1357-1807	2007-2312

Table 2: Location of the five downwind receptors used for flight planning and receptor flux calculations. Also shown are each receptor's mean BLB flux. Errors for BLB fluxes are based upon the uncertainty in CO_2 concentrations and boundary layer height.

Receptor	Latitude	Longitude	Mean Flux
Fraser Experimental Forest (FEF)	39.91	-105.88	-7.2 $\pm$ 5.4
Granby (GNB)	40.09	-105.92	-1.2 $\pm$ 3.1
South Northpark (SNP)	40.56	-106.18	-5.2 $\pm$ 3.7
Walden (WAL)	40.75	-106.27	-1.6 $\pm$ 7.1
Willow Creek (WIL)	40.36	-106.09	-13.2 $\pm$ 3.9

Table 3: The northern and southern extent (latitude, longitude) which determines the polygon sampled from CarbonTracker in the footprint analysis. The footprint is used to estimate the biosphere flux measured on each of the seven flight days analyzed (Table 1) .

Case	Date	N. Upwind	N. Downwind	S. Downwind	S. Upwind
1	1 Jun	42.5,-107.5	41.0,-105.5	39.0,-106.5	40.5,-108.0
2	15 Jun	41.5,-108.0	41.5,-105.5	39.0,-106.5	39.5,-107.5
3	21 Jun	42.0,-108.5	41.5,-105.5	39.5,-105.5	39.0,-109.0
4	18 Jul	40.0,-109.0	42.5,-105.5	39.5,-105.0	39.0,-108.5
5	1 Aug	42.0,-106.0	39.0,-104.5	40.5,-104.5	40.0,-106.5
6	3 Aug	40.0,-108.0	41.5,-105.5	40.0,-105.5	39.5,-107.5
7	9 Aug	40.0,-108.0	41.5,-105.5	39.5,-105.0	39.0,-107.5

Table 4: Location of the five sources used in the HYPACT simulations. Source numbers correspond to those in Figure 5.

Source	Latitude	Longitude
1	39.46	-108.57
2	40.17	-108.41
3	40.50	-108.09
4	39.53	-107.79
5	39.67	-106.94

Table 5: Estimates of the maximum boundary layer height, in meters, for the seven flight days analyzed (Table 1). Estimates are from NARR reanalysis data, vertical profiles of θ_v and q and from the bulk Richardson number ($Ri_c = 0.25$). Errors from NARR represent the 1-σ spatial variability. Errors from Ri_B were computed by changing the altitude bin size and Ri_c. Uncertainty in θ_v/q boundary layer heights are twice the bin size, instrument error is negligible Combined uncertainty is 25%.

Case	Date	NARR	θ_v/q	Ri_B
1	1 Jun	2381 ± 883	2176	1052 ± 492
2	15 Jun	3318 ± 1208	2930	3196 ± 196
3	21 Jun	4551 ± 1676	3574	3648 ± 512
4	18 Jul	3220 ± 1205	2970	3649 ± 598
5	1 Aug	2938 ± 1064	2725	1200 ± 394
6	3 Aug	2641 ± 848	2675	1900 ± 454
7	9 Aug	3335 ± 1312	3020	3349 ± 98
Mean		3198	2867	2571
Std. Dev.		696	422	1152
% Uncertainty		36	4	25

Table 6: BLB flux estimates, in μmol m^{-2} s^{-1}, from ACME07. Shown are the BLB fluxes using the various estimates of boundary layer heights (NARR, θ_v and q, and Ri_B). BLB Flux errors were calculated based upon the uncertainty in CO_2 concentrations and boundary layer height.

Case	Date	NARR	θ_v/q	Ri_B
1	1 Jun	-7.5 $\pm$ 2.6	-6.9 $\pm$ 2.3	-3.2 $\pm$ 1.1
2	15 Jun	-1.4 $\pm$ 2.6	-1.4 $\pm$ 2.2	-1.4 $\pm$ 2.5
3	21 Jun	-12.0 $\pm$ 3.6	-9.6 $\pm$ 2.8	-9.8 $\pm$ 2.9
4	18 Jul	-7.8 $\pm$ 2.6	-7.2 $\pm$ 2.3	-8.92 $\pm$ 3.0
5	1 Aug	-7.1 $\pm$ 2.2	-6.7 $\pm$ 2.0	-8.0 $\pm$ 1.0
6	3 Aug	-5.0 $\pm$ 2.2	-5.0 $\pm$ 2.2	0.2 $\pm$ 1.6
7	9 Aug	-10.4 $\pm$ 2.7	-9.3 $\pm$ 2.3	-10.5 $\pm$ 2.7
Mean		-7.3	-6.6	-6.0
Std. Dev.		3.5	2.8	4.4

Table 7: Daytime regional flux estimates, in μmol m^{-2} s^{-1}, from ACME07. Shown are the BLB receptor averaged fluxes and flux estimates from the CarbonTracker (CT) footprint analysis and NWR. BLB Flux errors were calculated based upon the uncertainty in CO_2 concentrations and boundary layer height. Errors from CarbonTracker represent the 1-σ spatial variability.

Case	Date	Receptor	CT Footprint	NWR
1	1 Jun	-9.9 $\pm$ 2.7	-12.5 $\pm$ 4.6	-8.9
2	15 Jun	-0.3 $\pm$ 2.5	-11.4 $\pm$ 3.3	-4.6
3	21 Jun	-8.9 $\pm$ 4.1	-12.3 $\pm$ 6.8	-2.5
4	18 Jul	-7.8 $\pm$ 2.5	-1.2 $\pm$ 1.7	-4.9
5	1 Aug	-10.8 $\pm$ 2.2	-4.3 $\pm$ 5.3	-6.9
6	3 Aug	-6.1 $\pm$ 2.3	-2.3 $\pm$ 3.0	-6.8
7	9 Aug	-9.0 $\pm$ 2.8	-4.7 $\pm$ 1.3	-4.6
Mean		-7.5	-7.0	-5.6
Std. Dev.		3.5	4.9	2.0